Single Molecule Measurements of Titin Elasticity

Kuan Wang[‡]*, Jeffrey G. Forbes[‡†], and Albert J. Jin[‡#]

[‡]Laboratory of Physical Biology, NIAMS, NIH, Bldg. 6/Rm 408, Bethesda, MD 20892, USA; [†]Department of Chemical Engineering, University of Maryland, College Park, MD 20742-2111, USA; [#]Division of Bioengineering & Physical Science, ORS/OD, NIH, Bldg. 13/ Rm. 3N18, Bethesda, MD 20892, USA.

*Corresponding author. E-mail: wangk@exchange.nih.gov, Tel: (301) 496-4097, Fax: (301) 402-8566. http://www.nih.gov/niams/about/irp/lpbintro.htm

Running Title: Elasticity of Titin

Key words: atomic force microscopy; AFM; laser optical trap; LOT; polymer elasticity; biological forces; muscle protein.

Table of contents {correct page numbers-on proof & production}:

Abstract

Titin, with a massive single chain of 3-4 MDa and multiple modular motifs, spans the half-sarcomere of skeletal and cardiac muscles and serves important, multifaceted functions. In recent years, titin has become a favored subject of single molecule observations by atomic force microscopy (AFM) and laser optical trap (LOT). Here we review these single titin molecule extension studies with an emphasis on understanding their relevance to titin elasticity in muscle function. Some fundamental aspects of the methods for single titin molecule investigations, including the application of dynamic force, the elasticity models for filamentous titin motifs, the technical foundations and calibrations of AFM and LOT, and titin sample preparations are provided. A chronological review of major publications on recent single titin extension observations is presented. This is followed by summary evaluations of titin domain folding/unfolding results and of elastic properties of filamentous titin motifs. Implications of these single titin measurements for muscle physiology/pathology are discussed and forthcoming advances in single titin studies are anticipated.

1. Introduction

Although striated muscle research has had hundreds of years of history, the classic two-filament sarcomere consisting of myosin thick filaments and actin thin filaments as the force-generating unit has only been known for less than 50 years [as reviewed e.g. in (Huxley, 1990)]. The discovery of the giant protein titin (also known as connectin) over 20 years ago added a third filament system that is crucial to the sarcomeric elasticity, structure and function (Fig. 1) (Maruyama *et al.*, 1981; Wang *et al.*, 1979). Proteins of the titin family are the longest single polypeptide chains currently known and have a molecular mass in the range of 3-4 MDa. The complete cDNA sequence of human cardiac titin was first reported by Labeit and coworkers (1995), and intriguing tissue- and species- specific alternative splicing pathways of titin have now emerged (Freiburg *et al.*, 2000; Labeit and Kolmerer, 1995) (Fig. 2A). Human titin gene has 234 exons, the largest number in a single human gene (Venter, *et al.*, 2001). Isolated titin is a monomer that is long, slender and flexible. Its conformational malleability can be seen in its EM images in Fig. 3. When the molecules are relaxed they take on a highly convoluted configuration (Fig. 3A). However, titin can be easily entangled and readily stretched by meniscus forces while preparing the EM samples (Fig. 3B-E). The knowledge of modular motifs in titin has accelerated more targeted studies *via* both the traditional myofibril mechanics/immunolocalization methods and various single molecule techniques, yielding an ever-increasing body of insights. These extensive studies in recent years have solidified our knowledge of the multifaceted roles that titin plays in the sarcomere [see e.g. recent reviews (Horowits, 1999; Maruyama, 1997; Trinick and Tskhovrebova, 1999; Wang, 1996; Wang, 1999)].

This review article focuses on titin as the source of passive tension (elasticity) in the sarcomere *via* its elastic properties as provided by single molecule investigations. Passive tension refers to the mechanical force exerted by the sarcomere against stretching, in contrast to the active force produced by actin/myosin interactions that is driven by ATP hydrolysis. Titin was quickly established to be the major filament that supports passive tension in the sarcomere by linking the tips of myosin filaments to the Z-line via several serially connected elastic segments with distinct extensibility (Fig. 1). The elasticity of titin filaments *in situ* was predicted at the time of its discovery as a major myofibrillar component (Maruyama *et al.*, 1981; Wang *et al.*, 1979). A strong correlation between the passive tension and the extension of titin was established by a number of studies using immunoelectron microscopy and the translocation of unique titin epitopes in sarcomeres (Horowits *et al.*, 1989; Maruyama, 1994; Trombitas and Pollack, 1993; Wang *et al.*, 1991). The pivotal role of titin in muscle elasticity was also

supported by studies using protease digestion and low doses of ionizing radiation. Both of these techniques readily destroy the passive tension of muscle fibers in proportion to the degradation of the high-molecular-weight titin (Funatsu *et al.*, 1990; Horowits *et al.*, 1986). Furthermore, titin was found to contribute the majority of the passive tension in muscle compared with other force-bearing filaments (e.g. collagen and intermediate filaments) in the normal working range of muscle extension (Granzier and Irving, 1995; Granzier and Wang, 1993b). These results prove conclusively that, by acting as an elastic connector between the tip of thick filaments and the Z-line (i.e., the I band of the sarcomere), titin imparts elasticity and structural integrity to the sarcomere.

Quantitatively, sarcomere passive tension and *in situ* titin extensibility can be scaled across multiple muscle tissue types to a single master relationship by the length of such elastic connectors in the sarcomere, which in turn is determined by the length of the titin isoform(s) selectively expressed in each muscle (Fig. 2A). The segmental extension model of titin elasticity thus emerged from such intriguing correlation of titin size isoforms and the elastic limits (yield points) of each muscle tissue (Wang *et al.*, 1991) (Fig. 2B). In the I-band region, where titin extends during passive force development, titin is comprised of serially-linked motifs of three types: (1) The folded 100-residue modular repeats of immunoglobin (Ig) or fibronectin III (Fn3) domains, (2) a unique PEVK motif consists of 70% of proline, glutamate, valine, and lysine residues, and (3) the N2-A or N2-B insert (Labeit and Kolmerer, 1995). Tissue- and species-specific alternative splicing extensively alters the expression of these motifs (Freiburg *et al.*, 2000; Labeit and Kolmerer, 1995). The cardiac I-band titin is comprised of two sub-types, termed N2-B and N2-BA, both having the N2-B titin insert that is a few hundred amino acid residues longer than the N2-A titin insert and a PEVK motif that is as short as 163 amino acids. The skeletal titins, on the other hand, all have much longer poly-Ig motifs with up to 53 additional Ig modules, N2-A insertion, and much longer PEVK motifs with up to 2174 residues in human soleus muscle (Fig. 2A). During the stretching of sarcomeres, the poly-Ig motifs of titin first straighten and produce a very low restoring force. The unique segments, PEVK and N2-B or N2-A, then extend greatly, producing an essentially exponentially rising force. Upon reaching the yield point force, the inextensible titin segment in the A band dislodges from the thick filaments, becomes extensible, and then the passive force levels off (Figs. 1A and 2B). The major defining characteristics of each tissue-specific force-extension curve are the total length of the extensible Ig-motifs which sets the length SL_E-SL_O for initial low force-low extension region; the total length of the unique sequences (PEVK plus N2-B and/or N2-A),

which sets the length SL_Y-SL_E; and the intrinsic extensibility of each sequence motifs of PEVK/N2 which sets the force scale for the exponential rising force region.

The strength of titin/thick filament interactions (F_Y) determines the elastic limit (SL_Y) and further stretching beyond the yield point only detaches an increasing number of the Ig and Fn3 domains that were originally adhered to the myosin filaments, without further increase of force. Thus the recruitment of titin domains from the thick filament region acts as a mechanical delimiter to prevent the massive unfolding of its Ig and Fn3 domains (Figs. 1 and 2B) while maintaining the structural continuity and preventing the detrimental fracturing of the sarcomere. The segmental extension and sequential recruitment of segments/motifs of titin in the sarcomere form a scaling base for unifying passive tension characteristics of skeletal, cardiac and insect flight muscles. The recent demonstration by immuno-staining that each of the PEVK, N2A and B, and Ig segments extend as distinct segments support the soundness of this sequential extension/recruitment concept (Granzier et al., 2000). This model also provides the framework to integrate the single titin elasticity measurements and sarcomeric mechanics/immuno-imaging observations of striated muscle.

In the balance of this review, we focus on single titin molecule extension studies and the resulting insights into titin elasticity. In Section 2, we provide some fundamental aspects of methods for single titin molecule investigations. First, we introduce the concepts of dynamic force and entropic spring models that are centrally relevant to titin behavior under extension. Two single molecule study techniques, atomic force microscopy (AFM) and laser optical trap (LOT), are then explained. Titin molecule sample preparation techniques are also discussed. In Section 3, we give a review of major publications on recent single titin extension observations, first in a chronological order, then in summary comparisons. In Section 4, we provide a more comprehensive evaluation of titin domain folding/unfolding observations in the context of protein folding and energetics. In Section 5, we summarize the elastic properties of filamentous titin motifs in relationship with cardiac and skeletal muscle elasticity in physiology/pathology, and provide brief concluding remarks on forthcoming advances.

2. Methods - single molecule extension

The last decade of the twentieth century was a time of rapid advances in the study of single molecules by a variety of methods, including fluorescence, electron microscopy, laser optical trap (LOT), and scanning probe microscopy such as atomic force microscopy (AFM). One area of investigation that has been particularly fruitful is the study of the mechanical

properties of single molecules such as DNA, modular proteins, and synthetic polymers. These experiments have yielded exciting and novel information on the shape, dynamics and mechanical properties of individual molecules that previously could only be inferred from the average properties of polymers in bulk. From the pioneering work of Ashkin and colleagues (Ashkin, 1980; Ashkin, *et al.* 1986), LOT has been developed into a tool that can simultaneously manipulate multiple molecules individually, while accurately measure forces on the order of 1.0 pN (Block, 1995; Visscher and Block, 1998; Mehta *et al.*, 1999). AFM was invented a few years later (Binnig *et al.*, 1986; Hansma *et al.*, 1988) and is now recognized as a powerful imaging and force measurement tool with a large dynamic range, from Ångstroms to microns, and with utility in high vacuum, at cryo to high temperature, and in aqueous environments. Titin is an ideal subject for mechanical studies, because it plays a mechanical role in muscle and, due to its large mass (3-4 MDa) and extended structure of *ca.* 1 μm in length, it can be more easily manipulated than smaller molecules. In 1997, two LOT studies of titin were reported (Kellermayer *et al.*, 1997; Tskhovrebova *et al.*, 1997). Around the same time, the first AFM measurement of titin elasticity was reported (Rief *et al.*, 1997a). These studies set the stage for an explosive growth of interests and insights of how external force alters the rates and pathways of folding and interactions of proteins. We will first describe the conceptual basis of the interplay between external force and the rate and energetics of protein folding and interaction. We will then critically evaluate the observations and data interpretations of titin elasticity based on these two single molecule techniques.

2.1. Molecular forces and energy surfaces

While there is a myriad of ways to apply forces to a bulk material, currently only tension and torsion (Strick *et al.*, 2000; Tsuda *et al.*, 1996; Yasuda *et al.*, 1996) can be applied to single molecules. Since titin has little torsional rigidity (Fig. 3), only tension is applicable and transmitted along titin. In contrast, torsion is relevant to DNA and protein filaments with greater flexural rigidity. The application of tension to a molecule can stretch the molecule, break down intramolecular folds, rupture protein/protein or protein/ligand interactions, and weaken or rupture the attachment to the force-measuring instrument. Thus, specific application of tension to single molecules allows numerous important biological observations to be made.

The force-induced rupturing of protein/ligand interactions or protein unfolding may be conceptualized on the basis of transition-state theory that describes chemical or physical reactions as taking place on a potential energy surface with many possible reaction paths from reactants to products. Different paths that any given reaction may take will have different barrier heights and possibly local minima on the reaction surface. The most likely path, i.e. the one with the lowest barriers, will be a saddle point on the energy surface. An example of such a path on the surface with one intermediate state is represented in Fig. 4A. The bound or folded state is in the deep well and the unbound or unfolded state is where the energy is zero to the right. For simple reactions such as two atoms reacting to form a diatomic molecule, the length scale of the reaction coordinate can be directly related to bond length. For complex bonding surfaces as those found in protein-ligand complexes and in folded proteins, a direct and simple correlation between the molecular distance and the reaction coordinate does not exist. The length of the reaction coordinate may give an indication of the nature of the transition state. For a shorter reaction width, the transition state is more like the bound state than the unbound state. Conversely, a longer reaction width indicates a transition state that is more like the unbound products.

In biological systems, the macromolecules themselves are covalently linked polymers that form complex folded conformations and interact with one another and the water molecules that surround them through a network of non-covalent interactions. These interactions are complex and dynamic, associating and dissociating at all times, with the molecular motions significantly damped by the viscous environment. Mechanical stress alters the magnitude and the rate of interactions, with a tendency toward the disassembly of the structure when an external stretching force is applied. This bias towards bond rupture by the application of stretching force was first discussed by Bell in his model based on the kinetic theory of the strength of solids (Bell, 1978). Evans and Ritchie have extended the work of Bell to the dynamic application of force that occurs frequently in biological systems (Evans, 1998; Evans, 1999). They applied Kramer's theory of

chemical kinetics in a Brownian field (Kramers, 1940) to the bond strength of biological interactions in water. The viscous damping of the molecular motion leads to bond lifetimes at least 1000-fold longer than that predicted from the bond excitation frequencies used in Bell's theory. The bond lifetime in Bell's theory is written as,

$$\tau = \tau_0 e^{(E_0 - \gamma f)/k_B T} \tag{1}$$

where E_0 is the bond energy, f is the applied force per bond, τ_0 is the reciprocal of the bond vibrational frequency (10^{-13} s), and γ is a characteristic of the solid. Bell postulated that this formula could be applied to receptor-ligand pairs if $\tau(f=0)$ is equivalent to the inverse of the off-rate of the ligand and that γ must be approximately r_0 (the distance between the receptor and ligand) so that $\tau = \tau_0$ when $f = E_0/r_0$. During the application of tension upon the interface, the force is assumed to act along the reaction coordinate, x, from 0 at the bound or native state to reach x_u, at the transition state at the top of the energy barrier (Fig. 4A). This model implies that that the bond lifetime should decrease exponentially with increasing force:

$$\tau(f) = \tau_0 e^{(-f \cdot x_u)/k_B T} \tag{2}$$

where $k_B T$ is the thermal energy scale. From the above equation, it is seen readily that the bond lifetime varies as a function of the applied force, f, and the width of the reaction coordinate, x_u. As the width of the reaction coordinate increases, the bond lifetime decreases more rapidly for a given applied force. In general, receptor-ligand bond lifetimes can range from milliseconds to hours.

The decrease in bond lifetime with applied force results directly from the effect the force has upon the reaction coordinate. For complex molecular systems, the attachment point for applying force to the molecules may not allow for force directly along the reaction coordinate.

When a mechanical force is applied at an angle θ to the reaction coordinate, the reaction surface potential is distorted and linearly tilted by $-fx\cos\theta$, with $f\cos\theta$ being the force component along the relevant reaction coordinate (Fig. 4A). The effect of this tilting of the potential is that the energy barriers are lowered, the probability of crossing increases, and therefore the reaction rate increases. The increased probability leads to an increase in the rate of bond rupture. For a three state unbinding reaction illustrated in Fig. 4A, the outer barrier determines the crossing probability under smaller force, and the relevant width of the reaction coordinate is large. However, under larger forces the inner barrier becomes higher than the outer one and determines the crossing probability. So the width of the reaction coordinate is smaller at higher force.

In the analysis of Evans and Ritchie (1997), the activation energy for bond rupture, rather than the bond free energy, is the main determinant of the bond strength under a mechanical load. Also in biological applications, the applied force usually varies with time. Evans and Ritchie's analysis showed that the weak non-covalent interactions found in protein-ligand interactions, as well as those involved in protein folding would be sensitive to the loading rate of the applied force. The probability of bond rupture under a given load is the product of the off-rate under the load and the likelihood of bond survival under the load. As the load increases with time, the off-rate increases in time and the likelihood of bond survival decreases in time, which leads to a peak in the statistical distribution of rupture events (Fig. 4B). The peak in the distribution is regarded as the bond strength and it increases with higher loading rates. The width of the distribution also increases with higher loading rates (Fig. 4B). The bond strength varies linearly with the log of the loading rate, while the slope depends upon both the bond lifetime and the width of the reaction coordinate (Fig. 4C). Because the width is in the exponent of the bond lifetime function, small changes in the width can have a large effect. For a given bond lifetime, an increase in the width of the reaction coordinate will decrease the slope of the rupture force *vs.* log(loading rate) plot (Rief *et al.*, 1998). Therefore a larger reaction coordinate width reduces the sensitivity of the

interaction to the loading rate. This difference in sensitivity to applied force of homologous proteins with similar folding pattern and stability is therefore a manifestation of different dynamic force unfolding reaction widths. For a protein to withstand unfolding by the rapid application of force, it would require a short reaction width. If a protein is to unfold over a large range of loading rates, it has to have a wide reaction width so that it will unfold at high rates and low forces. The sensitivity of bond strength to the folded lifetime has been demonstrated by Monte Carlo simulations of the distribution of unfolding forces for an Ig domain (Fig. 4D). While the shape of the distribution does not change significantly from varying the folded lifetime over two orders of magnitude, the simulated bond strength changes significantly. The experiments behind Fig. 4D and their interpretation will be discussed more fully in section 3.2.

For many biological processes, the energy landscapes can be expected to be more complex due to the large number of interactions in these biological interfaces. These barriers can have different positions along the reaction coordinate, i.e. widths and heights (Fig. 4A). At low loading rates, the unbinding kinetics is dominated by a barrier farthest from the potential well. As the loading rate is increased there is a change of the potential surface and crossover to the kinetics being dominated by the inner barriers. The force *vs.* loading rate plot for biotin-avidin best demonstrates this behavior (Fig. 4C), where three different slopes indicate three different reaction widths in the unbinding reaction pathway (Merkel *et al.*, 1999). The two inner barriers (higher force loading) at 0.12 nm and 0.3 nm compare well with the position of prominent transition states in molecular dynamics simulation of the unbinding of biotin from avidin at *ca.* 0.1 nm and 0.4 nm (Izrailev *et al.*, 1997). The outer barrier as determined by dynamic force spectroscopy is at 3 nm, whereas the last transition in the molecular dynamics calculations is seen at 1.4 nm. This two-fold difference in the outer barrier may result from the interaction of the biotin with peripheral, flexible loops at the mouth of the binding pocket (Chu *et al.*, 1998). The molecular dynamics calculations are made at much shorter time scales and much higher loading

rate than in real physical measurements. The loop dynamics at the picosecond time scale used in the molecular dynamics calculations are very different from those at the millisecond time scale in force spectroscopy. These results indicate that dynamic force spectroscopy of biological interactions can be a powerful tool for revealing subtleties of the interaction potential which cannot be probed by other experimental means. While a strict physical interpretation of the reaction surface may not be accessible without molecular modeling, the presence of hidden barriers can provide insights into the binding mechanisms that may be biologically relevant. Strunz *et al.* (2000) have recently modeled the energy landscape during force-induced dissociation of a macromolecular interaction. They found that even a single intermediate state leads to various, complex dependencies of the bond lifetime on the applied force.

2.2. Elasticity models for titin

Several evolving models of molecular elasticity have been applied to describe titin extension and sarcomere elasticity (Fig. 5). The original segmental extension model by Wang and coworkers proposed that titin *in situ* extends in segments as a dual/multiple stage spring. The extension of the I-band segment titin led to the exponential rising of tension (ERT) model of sarcomere passive force (Granzier and Wang, 1993b; Wang *et al.*, 1991) (Table 1). ERT of muscles that expressed different titin isoforms can be scaled by the I-band titin strain as, $\varepsilon \equiv (TL_E - TL_{EO})/TL_{EO}$ where the subscripts denote the titin length (TL) at a given extension, (*EO*) denotes the onset of exponential extension, (*O*) denotes the rest length, E_0 and α are two adjustable parameters.

Despite the success of this theory in predicting the tension-length curves of various muscles, sarcomere mechanics provides only a limited view of the full range molecular elasticity of titin. Experimentally, it is difficult to apply a large force at will to titin in the sarcomere, because the applied force cannot exceed the yield point value that starts to dislodge titin from its attachment to the tip of thick filaments. This yield point force is estimated to be *ca.* 45 pN per titin for rabbit psoas muscle (Wang *et al.*, 1991). It is equally difficult to impose small forces of less than a few pN per titin in the sarcomere because of competing factors such as the weak crossbridges between actin and myosin in non-activating conditions (Granzier and Wang, 1993b).

For these technical reasons, single molecule measurements with forces as high as several hundred piconewtons are more versatile and greatly expand the force-extension range of titin.

Two polymer-based elasticity models (Fig. 5A), the worm-like chain (WLC) and the freely-jointed chain (FJC), have been applied with varying degrees of success to explain the force –extension behaviors of single titin molecules. The WLC model describes a semi-flexible rod undergoing entropy-driven configurations with two parameters, the persistence length, L_p, and the total chain contour length, L_o (Marko and Siggia, 1995; Ortiz and Hadziioannou, 1999) (Table 1). Recent enhancements developed in the context of DNA elasticity also include enthalpic stretch contributions *via* an elastic force constant, K_o (Bouchiat *et al.*, 1999; Wang *et al.*, 1997b). The current fitting equations, due to simplifying approximations, may deviate from exact solution by 10% in some ranges of extension. Adopting this model allows for the determination of the elastic persistence length, L_p. A larger L_p indicates that the chain is stiffer with fewer bending and orientational fluctuations. The elastic modulus, K_0, determines the degree to which the polymer chain can be extended under the applied force and represents an enthalpic contribution to the elasticity. A smaller K_0 represents a more extensible polymer chain.

The freely-jointed chain (FJC) model is based on polymer chains with a linear string of rigid rods rotating freely at the joints and with no interactions between the rods. The elastic parameters are the Kuhn segment length L_K and the total polymer length L_o. For similar filaments, $L_K = 2L_p$ gives a good first approximation (Table 1). This model has also been enhanced to include an elastic stretching term, K_o (Muniz *et al.*, 1999; Ortiz and Hadziioannou, 1999).

It is useful to note that, in this context, stiffness refers to the resistance to bending, not to extension, as it is generally used in muscle mechanics. The elasticity parameters, L_K and L_p, denote the bending configurational freedom for the filamentous chain (Fig. 5A). For an extended chain with larger end-to-end distance, the entropy of the chain from backbone bending is smaller and, hence, its free energy is higher than that of the collapsed chain. It therefore takes force to stretch the chain as work is needed to make up for the free energy increment. A smaller L_K in the FJC or L_p in the WLC allows for more bending fluctuations of an under-stretched filament, which results in a decrease in the free energy of the polymer chain and it behaves as a stiffer entropic spring. In the original WLC and FJC models, the total length of the chain backbone does not change during stretching; the inclusion of the K_o modulus gives an approximation for small backbone extension when the entropic force is transmitted along the chain. One should also note that for both of these phenomenological models, chain segments are assumed not to interact with

each other, i.e. no tendency for self-organization or self-avoidance. All models predict titin as a linear spring at small extensions and as a nonlinear spring with rapidly rising tension at higher extensions. Indeed, quantitatively there is very little distinction between these models with the limited force/extension range encountered in the sarcomere. This point is illustrated in Fig. 5B, where five sets of elastic parameters from three models all led to force-extension curves that are almost completely overlapping at fractional extensions below 0.8. This is the degree of extension of titin in the normal range of sarcomere extension. Although single molecule measurements now begin to favor the WLC model, as it provides structural insights into the molecular elasticity of titin (See Section 5), distinctions among the three models are largely superficial in the context of sarcomere elasticity.

2.3. AFM and LOT techniques

Direct measurement of forces within and between molecules has remained an intractable problem for several reasons: attachment of molecules, measurement of forces in the piconewton (pN = 10^{-12} N) range, and reproducible mechanical motion on the sub-nanometer scale. The last two problems were solved by the invention of the AFM and LOT. A comparison of the major features of these techniques is presented in Table 2 and they will be described in more detail below. The solution to the attachment problems follows from the materials used in the measuring techniques: glass, silicon, silicon nitride, and polymer microspheres. Many chemical methods have been successfully developed for immobilizing proteins and other types of polymeric materials on these types of surfaces.

2.3.1. Atomic force microscopy

Considering the ability of the AFM to sense directly the topology of atoms, molecules and cells, its design and operation are surprisingly simple. An AFM has four basic components: a microcantilever for sensing forces; a means of detecting cantilever deflection; a piezoelectric system for moving the tip in *X*, *Y*, & *Z* coordinates at atomic resolution; and a computer control system (Fig. 6A). In a typical commercial system, the cantilever is microfabricated from silicon nitride or silicon using semiconductor fabrication methods. The cantilever is mounted on a tip holder that is mounted on a tubular piezoelectric element for moving the cantilever over the surface. The cantilever motion is detected by an optical lever method, where a laser is bounced off of the cantilever into a split photodiode. The photodiode allows bending motion of the

cantilever to be detected to better than 1 Å. The cantilever behaves as a Hookian spring with a force constant, k, on the order of 0.01 – 1 N/m. The force on the cantilever may be determined directly from the deflection of the cantilever and the force constant of the cantilever using Hooke's law, $F = kx$. To image a sample, the tip is brought into contact with the surface at a loading of several hundreds of pN to several nN (1 nN =1000 pN=10^{-9} N). The cantilever is then rastered over the sample while maintaining a constant force applied to the sample. The motion of the tip holder normal to the surface that is required to maintain a constant force yields a topographic image of the surface. The AFM is capable of measuring forces in a similar manner where the tip holder is moved up and down and the deflection of the cantilever is measured.

Since its inception in 1986 (Binnig *et al.*, 1986), the force measuring capabilities of the AFM have been touted as one of the most significant advantages of this new technique. It was estimated early on, that forces as small as 0.01 pN could potentially be measured with the AFM. Extensive effort for over a decade has shown that the practical limitation of this technique is on the order of 10 pN (Viani *et al.*, 1999a). Although other techniques can be used to measure smaller forces, the AFM has the advantage of a large dynamic range in force measurement. With a single cantilever, forces ranging from tens of piconewtons to over a nanonewton can be measured easily. Even larger forces can be measured with stiffer cantilevers. Much of the early work on force measurement with the AFM dealt with interactions between the tip and surface, and the visco-elastic properties of different materials. Measurements of the interaction forces between single molecules were first reported in 1994 with the studies of the interaction between avidin and biotin (Florin *et al.*, 1994; Lee *et al.*, 1994), and DNA oligomers (Lee *et al.*, 1994). Since these first unbinding force measurements, many other systems have been studied: antibodies, insulin dimers, metal ligands, among others. The first extension of a single polymer chain with an AFM was reported by Hinterdorfer *et al.*, (1996) where they tethered an antibody and its antigen *via* a polyethylene glycol (PEG) linker. While the elastic property of PEG was secondary to their study of the antibody–antigen interactions, it demonstrated the potential for stretching polymers with the AFM. In 1997, Rief and coworkers reported the first study of the elastic properties of a polymer, where they stretched dextran with an AFM (Rief *et al.*, 1997b).

In the interaction force experiments, one of the binding partners was attached to the AFM tip and the other to the surface. When the tip is brought into contact with the surface, the receptor and ligand bind. Upon retraction of the tip from the surface, the adhesion of the receptor and ligand causes the tip to adhere to the surface, which is detected as a negative deflection of the cantilever. In the polymer extension experiments, the entropic elasticity of the polymer tethering

the tip and the substrate causes the cantilever to bend towards the substrate. When the force applied by the bending of the cantilever exceeds the interaction or the tethering force, the cantilever snaps back to its equilibrium position.

The distance the cantilever bent from its equilibrium position is proportional to the force. The proportionality constant is the Hooke's constant for the cantilever. This parameter can be estimated from the dimension of the cantilever using the Young's modulus of the material. However, this is more difficult than it would seem in practice, because the silicon nitride cantilevers are formed by chemical vapor deposition, which results in a non-stoichiometric material for which there is no single Young's modulus. Several methods have been developed to work around this problem (Sader *et al.*, 1999; Sader *et al.*, 1995); however, experimental determination of the force constant is preferable. Two reliable calibration methods are based on the added mass approach (Cleveland *et al.*, 1993) and the thermal fluctuation approach (Hutter and Bechhoefer, 1993). The latter method has been shown to yield results similar to the other methods (i.e. with less than about 10% discrepancy), as well as working in liquid and requiring no additional manipulation of the cantilever (Butt and Jaschke, 1995; Florin *et al.*, 1995).

2.3.2. *Laser optical trap*

The laser optical trap (laser tweezers) technique is now recognized as a powerful, non-invasive force measurement tool that complements the AFM in its force range and its utility in aqueous environment (Svoboda and Block, 1994; Visscher and Block, 1998). The optical trap is able to apply force from near 0.1 pN to hundreds of pN to a particle by the radiation pressure from the photons traveling through the particle (Ashkin, 1992; Ashkin, *et al.* 1986). The theory of the optical forces in laser tweezers has been well explained in a number of recent reviews (Ashkin, 1992; Block, 1992; Svoboda and Block, 1994; and other chapters in this two volume series). Briefly, an optical trap utilizes the gradient force, which draws objects with an index of refraction higher than the surrounding medium towards the high intensity region, and objects of lower index of refraction towards the low intensity region (Ashkin, 1992). Thus, counting only the gradient force, the focal point of a light beam through microscope objective is a three dimensional trap for objects with their index of refraction higher than the surrounding medium. Because the photons also exert scattering force on the object in the forward direction of the beam, a true 3D trap formed by a single laser beam must have tight focus in the axial direction so that the gradient force overcomes the scattering force to prevent the object from being ejected forward (Ashkin, *et al.* 1986; Svoboda and Block, 1994). To achieve such a tight focus, the laser beam is

usually focused through a high numerical aperture microscope objective and the particle becomes trapped in the beam near the focal point. Figure 6B shows a simplified schematic of a typical laser trap experiment. The optical microscope, being an integral part of LOT, allows the visualization of the particles being manipulated by the force trap. Usually latex or polystyrene spheres on the order of 1 – 3 μm in size are used for applying force to molecules. The large size of the particles needed for effective trapping can cause problems with applying forces to small molecules, but this is less of an issue for micron long polymers such as titin and DNA. The force applied to the particle is proportional to the power incident on the particle (Ashkin, 1992). While high power lasers are readily available, the practical upper limit is set by the amount of heat deposited into the sample and radiation damage. A temperature rise of 1.7°C/100 mW of laser power at the sample was estimated in one experimental setup using a 1064 nm laser (Kuo, 1998). Photon induced radiation damage can also be a major problem for many sensitive biological processes. Recent efforts have sought to reduce such problem by using selected photon wavelengths including the infrared wavelength of 1064 nm produced by the common and economical continuous-wave (CW) diode-pumped Nd:YAG laser (Neuman, *et al.*, 1999). Force is measured by adjusting the trap to have a low stiffness, typically on the order of k =0.0002 N/m. When the position of the trap is moved a distance d a force proportional to kd will be exerted on the particle and the polymer attached to it.

Accurate force measurements require that the laser optical trap be carefully calibrated, preferably at each session, which can be a challenging task (Dai and Sheetz, 1998; Svoboda and Block, 1994). The force induced onto a dielectric sphere by the change of the momentum of the incident photons depends critically on photon field gradient, the index of refraction of the sphere and surrounding medium and various geometric factors; so theoretical calculations are often not precise (Ashkin, 1992). The refraction of the incident laser beam, and the concomitant shift in the position of the beam leaving the trap have been used for calibrating the trapping force of a laser trap (Smith *et al.*, 1996). However, this method is difficult to perform in practice. In most calibration setups, the amount of force exerted on the sphere is calculated through the application of Stoke's Law, within its applicable range (Dai and Sheetz, 1998; Svoboda and Block, 1994). Stoke's Law relates the flow velocity of a fluid around a particle to the force exerted on the particle by the equation,

$$f = 6\pi \cdot r\eta \cdot v \qquad (3)$$

where *r* is the radius of the sphere, η is the viscosity, and *v* is the flow velocity. An important caveat of this method is that the fluid must flow smoothly around an object with no turbulence, i.e. a laminar flow. For particles on the order of several microns in size, the laminar flow requirement limits the force on the particle to about 10 nN, which is adequate (Gittes and Schmidt, 1998; Svoboda and Block, 1994). The LOT is calibrated by trapping the particle at a given laser power and then increasing the flow around the particle either by moving the microscope stage back and forth or pumping fluid through the experimental cell at known rates. The particle under study must also be kept several microns (i.e. more than 5-10 times the bead radius) away from the surface of the flow chamber walls, so that the surface boundary effect is minimal. Both the laser field and the laminar flow will be perturbed if measurements are made too close to the glass surface (Dai and Sheetz, 1998; Gittes and Schmidt, 1998). The flow velocity at which the particle is displaced from the trap is then used in Stoke's equation to calculate the amount of force on the particle. For higher force applications, the laser power (I) is raised to increase the stiffness of the trap. It is assumed that the slope of the F *vs.* I plot at low power is the same as that at high power and the trapping force is simply extrapolated. Because a LOT trap is three-dimensionally non-uniform, it is crucial to keep the path of the bead in actual measurements closely similar to that during calibration, or significant errors may arise (Stout and Webb, 1998).

2.3.3. Application ranges of AFM and LOT

Both the AFM tip and trapped beads are subject to thermal motions due to collisions with the solvent molecules in the environment, which determines the measurement uncertainty. Both the AFM tip and the LOT bead are under a linear restoring force of the cantilever with respect to the Hookian spring constant *k*. As such, one has the thermal fluctuation limiting the position of the AFM tip via the equal partition of the thermal energy as (Gittes and Schmidt, 1998),

$$E_T \cong k_B \cdot T \cong k \cdot \langle \Delta z \rangle^2, \qquad (4)$$

where k_B is the Boltzman constant, T is the absolute temperature and $\langle \Delta z \rangle^2$ is the mean square amplitude of the thermal fluctuation of the tip position in the direction of cantilever bending, z. Thus, the measurement uncertainty in the position, $\sigma_Z \equiv \sqrt{\langle \Delta z \rangle^2} \cong \sqrt{k^{-1} \cdot k_B \cdot T}$, decreases with a stiffer cantilever or trap, whereas the uncertainty in the force, $\sigma_f \equiv \sqrt{\langle \Delta f \rangle^2} \cong k \cdot \sigma_Z \cong \sqrt{k \cdot k_B \cdot T}$,

increases with a stiffer cantilever or trap. This results in the thermal component to the signal-to-noise ratio of the force measurements being proportional to the square root of the cantilever or trap spring constant, $f/\sigma_f \propto \sqrt{k}$. The cantilever in typical AFM setups has a force constant, *k*, on the order of 0.01 – 1 N/m, this gives σ_f = 10 -100 pN and σ_Z = 1-0.1 nm. The corresponding trap force constant is about a thousand fold smaller and depends linearly on the applicable laser power. Thus, LOT has about 30 times lower noise in force, but simultaneously 30 times higher noise in spatial localization. The maximum force, on the other hand, is determined by the force constant times the maximum deflection of the cantilever in AFM or the gradient trap dimension in LOT, both of the order of 500 nm. Therefore, AFM can apply force up to hundreds of nN, whereas LOT can apply forces up to a few hundred pN. LOT is more suited for low force applications in pN range where spatial resolution needs not to be higher than a few nm; AFM is more suited for higher force applications in the tens to hundreds of pN range and where a spatial resolution of better than 1 nm is needed.

Much of the recent work on the unfolding of titin domains has been done on small proteins comprised of several domains that are 4 nm in length and with an extension force of hundreds of pN. The application range consideration above shows why the AFM is a more suitable technique than the LOT for such single titin studies. More systematic considerations of the thermal fluctuations in both LOT and AFM suggest that appropriate noise filtering can improve the precision of the force measurements (Gittes and Schmidt, 1998; Liu *et al.,* 1999; Svoboda and Block, 1994). Nevertheless, recent observations on the unfolding properties of titin domains have been made mostly with the AFM, and a small number of observations on the low-force behavior of longer titin segments with LOT techniques. As such, this review will concentrate more on the AFM results than on the LOT results. For applications in the pN force range, such as those involving molecular motors (e.g. Block, 1995; Wang, *et al.*, 1998), LOT is more suitable, and this application is more fully reviewed in the articles cited above and Visscher and Block, (1998).

2.4. Titin sample preparation

Successful single molecule force measurements require that the polymer or protein under study is pure, homogeneous and monodisperse. While it is often assumed that a pure polymer is homogeneous, titin from a single tissue source exists in several different isoforms with similar

molecular weights (Fig. 3A) (Freiburg *et al.*, 2000). In cardiac titin, the tandem Ig, PEVK and N2B regions are differentially expressed and the elastic response of titin resides largely in these regions. Heterogeneity in the elastic response of a population of polymers will be difficult to model. If multiple polymers are stretched, the force that each filament experiences will be divided by the number of filaments being stretched, if all are being stretched at the same rate. The problem is that not all of the polymers in an aggregate may even be under tension, and by interacting with those filaments under tension the overall elasticity will differ from the isolated polymer. Additionally, efforts must be taken to ensure that the measurements are not obscured by extraneous interactions. These extraneous interactions can arise from contamination of the surfaces used for immobilizing the polymer or protein, as well as non-specific interactions between the protein and substrate. A synopsis of the methods used in the titin extension experiments is given in Table 3.

2.4.1. Protein preparation

Verifying the purity of proteins and polymers is rarely as accurate or straightforward as with small molecules. The extremely large size of titin exacerbates this problem and special methods must be used for characterizing the size distribution and purity of the protein preparations (Wang, 1982). The AFM measurements on native titin (Rief *et al.*, 1997a) used bovine cardiac titin isolated as described by (Pan *et al.*, 1994). The laser optical trap measurements on native titin used rabbit back muscle (*Longissimus dorsi*) isolated as described by (Soteriou *et al.*, 1993). These procedures involve extraction of titin and myosin with a high salt buffer, followed by removal of the myosin by ion exchange or hydroxyapatite chromatography. Aggregated titin is then removed by gel filtration to yield monodisperse titin. The final preparation is mainly truncated titin, T2, (Fig. 1) where a portion of the amino terminus has been cleaved by proteolysis. In most cases T2 is also contaminated with titin binding proteins such as myomesin, M protein, attached at the carboxy-terminal or M-line end of titin. (Wang *et al.*, 1984) first demonstrated that hydroxyapatite chromatography can be used for removal of these M protein contaminations. Intact titin, T1, (Fig. 1) is apparently also present in minor amounts in T2 preparations, because a T1 specific monoclonal antibody, T12, was used successfully to immobilize the amino-terminal (Z-line) end of titin in the LOT experiments, as will be described below. The titin T2 preparation following gel filtration in high salt remains monomeric. However, it tends to aggregate at physiological and lower salt concentrations. Interestingly, T2 also tends to aggregate at the air/water interface of droplets (Wang *et al.*, 1984).

This tendency of titin to aggregate renders some uncertainty in achieving monomeric attachment of titin for single molecule extension experiments.

Most of the AFM measurements on titin have been made using recombinant fragments (see Table 3 and Section 3). These fragments were engineered with two cysteines on the carboxy-terminus for immobilizing on a gold surface, and the amino terminus carries a His_6 tag for purifying on a nickel-NTA column (Carrion-Vazquez *et al.*, 1999b; Rief *et al.*, 1997a; Rief *et al.*, 1998). The histidine tags allows for an easy one-column purification. These recombinant proteins have primarily been comprised of immunoglobulin domains. However, fibronectin domains have also been studied (Rief *et al.*, 1998).

2.4.2. Attachment of proteins in AFM

To study the extension of a single polymer with the AFM, the polymer must be fixed to the cantilever tip and a flat substrate (Fig. 7A). Ideally, the attachment would be at a known position on the polymer, which could be the ends. As is often the case, the ideal situation is not the easiest to attain, and it is possible to study the extension of polymers without knowing the attachment position. One successful method is to attach polymers or proteins to a flat substrate and then "grab" them with the tip. The mechanism of "grabbing" can be either covalent attachment or physisorption, *i.e.* adsorption via physical forces. The desired result is to grab a single protein rather than a large number of filaments. The sharp apex of the AFM tip limits the number of molecules that can attach to the tip. The attachment of single polymers to the sharp AFM tip is one of the fundamental advantages of the AFM in measuring the force properties of single polymers.

One way of affixing the polymer to the tip is to chemically cross-link it. A covalent bond will resist a force much larger than is required to stretch a polymer or unfold a small globular protein domain (Grandbois *et al.*, 1999). While most AFM cantilevers are made from silicon nitride, the substoichiometric nitrogen composition results in a partial silicon characteristic of the surface. The silicon on the surface can be oxidized to silica, which may then be readily functionalized with silanes. A large number of organosilanes with different functionalities are commercially available from several suppliers. Typically a trimethoxy or triethoxy silane with a functional group on a long linker is used. The silane may be adsorbed to the reactive silica surface either from a solution or the gas phase. Proteins may then be attached to the silated surface *via* traditional cross-linking methods, such as carbodiimides or glutaraldehyde. These

methods can be used to covalently attach antibodies to a substrate and tip for specific attachment of a protein for extension studies (Forbes *et al.*, 2000).

Many proteins adhere readily to glass, silica and mica surfaces. Bovine serum albumin (BSA) has been shown to bind irreversibly to glass and silica surfaces. This characteristic has been used in a number of force measuring studies with biotinylated BSA (Florin *et al.*, 1994; Rief *et al.*, 1997b). The biotinylated BSA is adsorbed to the surface and then streptavidin is bound to the immobilized BSA. This immobilized streptavidin may then be used for binding biotinylated proteins. The streptavidin/biotin interaction can withstand about 200 pN (Chilkoti *et al.*, 1995; Moy *et al.*, 1994) with multiple interactions increasing the force required to detach the biotinylated polymer. Many other proteins also adhere strongly to these surfaces. This robust adsorption of proteins to an AFM tip has been the primary method of fixing titin to the AFM tip for extension studies. In all of the AFM studies we will describe below, the titin or titin fragment was first adsorbed onto a surface and then the AFM tip was pressed into the surface to pick up the protein for extension. While the exact mechanism of this adsorption of protein to an AFM tip is not known, it appears that the amino terminus of the protein can be picked up, allowing for a known attachment position of the protein under study. However, random positions along the polypeptide are equally likely to be adsorbed.

Mica is an ideal substrate for imaging biomolecules, because it is atomically flat and many proteins adhere well to it. In fact, many of these proteins adhere so well to mica that they behave like an adhesive when an AFM tip is pressed into them. Rather than observing the extension of the polypeptide, the tip sticks more tightly to the surface than it does in the absence of the protein. This characteristic must arise from multiple, strong interactions between the mica and protein and between the tip and the protein. While these multiple interactions may be welcome in an imaging substrate, they are undesirable for polymer extension work. A surface that allows for a specific attachment or at least relatively few attachment points is needed.

Gold films have been shown to be suitable substrates for both imaging of proteins and for force measurement. When properly evaporated onto mica, gold forms atomically flat areas with the Au (111) structure (close packed) (Derose *et al.*, 1991; Zheng *et al.*, 1995). Gold can also be evaporated onto glass following a thin coating of chromium. Without the chromium, the gold will not adhere and will peel away from the glass. Gold evaporated onto glass will not be atomically flat, but will be dominated by small (~1 nm) globules whose size depends upon a number of factors. A perfectly flat surface is not necessary for force measurements and gold on glass is more readily prepared than gold on mica. Gold has the additional advantage that it can

be readily modified with alkane thiols, which form self-assembled monolayers that can have different functionalities. Thiols may also be used for passivating the gold surface to reduce further interaction between the protein and surface. Clean gold surfaces quickly adsorb compounds from the air, which renders the surface partially hydrophobic. All of the AFM studies of titin and titin fragment extension described below used a gold surface for immobilizing the protein. In the case of native titin, it may bind to the gold through surface cysteines or some physisorption process. In the work by Rief *et al.* (1997a), the native titin was stored at 0.5 mg/ml in phosphate buffered saline (PBS) with 0.5 mM dithiothreitol (DTT) and adsorbed onto the gold surface in PBS at a concentration of 10-100 μg/ml. Even with a dilution factor of 50, the DTT will be at a sufficiently high concentration that it will react with most of the available thiol reaction sites available on the gold surface. This indicates that native titin must interact with the gold surface through mechanisms other than just surface cysteines. All of the AFM studies of recombinant titin fragments have engineered the protein with two cysteines on the carboxy terminus of the protein (Carrion-Vazquez *et al.*, 1999b; Rief *et al.*, 1998). These recombinant proteins must be purified and stored in the presence of DTT or some other thiol reducing agent to ensure that the protein does not aggregate or form disulfide bonds. These thiol reducing agents must be removed from the buffer solutions just prior to reacting the protein with the gold surface.

2.4.3. Attachment of proteins in laser optical trap

As with the AFM, to stretch molecules with an optical trap, a single molecule must first be affixed to a stationary fixture at one end and a moveable fixture at the other. With the optical trap, the moveable fixture can be either a bead or a slide (Fig. 7B & C). The ideal "handles" are those specific to designated area of titin and strong enough to withstand the developed force. Kellermayer and colleagues (Kellermayer *et al.*, 1998; Kellermayer *et al.*, 1997) used the T12 antibody (Furst *et al.*, 1988) to affix native rabbit muscle titin to a 3 μm latex sphere. The T12 antibody binds about 100 nm from the Z-line end of titin, it therefore binds only to the contaminating T1 in the T2 preparation. Kellermayer and colleagues used several different methods to immobilize the M-line end of titin. A polystyrene bead was coated with either the T51 antibody to titin or myomesin (Kellermayer *et al.*, 1997; Obermann *et al.*, 1995). They also used 2 μm silica spheres, which had been coated with myomesin (Kellermayer *et al.*, 1998). The M-line binding sphere was held in a micropipette (Fig. 7B). The myomesin-silica spheres increased the chance of tethering the titin between the two spheres, but the beads often bound

non-specifically to various positions along the molecule. Tskhovrebova *et al.* (1997) have taken a different approach by immobilizing one end of the titin molecule on a glass slide that moved on a stage and using a latex microsphere in the optical trap as the stationary anchor, as well as for force sensing. They also used the T12 antibody to immobilize the Z-line end of titin and the AB5 antibody to immobilize the M-line end of the protein (Whiting *et al.*, 1989). Wang *et al.* (1997a) used stage affixed, streptavidin derivatized, latex beads to immobilize one end of biotinylated titin, and another streptavidin coated latex bead bound to the distal end of titin for the trap. The attachment sites were distributed randomly along the length of titin due to the biotinylation of titin. The high affinity and strong unbinding force of biotin/streptavidin, even in denaturing medium, allowed for specific attachment and made it possible to stretch titin in 8 M urea (Wang *et al.*, 1997a).

3. Measurements - single titin molecule extension

3.1. Chronological review

Atomic force microscopy imaging of titin was first reported in 1996 (Hallett *et al.*, 1996). Their work used the imaging ability of AFM and confirmed the filamentous conformation of titin molecules as seen in earlier EM studies (see Introduction and Fig. 3). As in the EM investigations, titin sample preparation appears to be an important factor in the outcome of the experiments.

For single titin elasticity, LOT investigations were first reported in meeting presentations in 1996 and early 1997 (Kellermayer *et al.*, 1997; Tskhovrebova *et al.*, 1996; Wang *et al.*, 1997a). Later in the same year three full publications appeared simultaneously, one in *Nature* (Tskhovrebova *et al.*, 1997) and the other two in *Science* (Kellermayer *et al.*, 1997; Rief *et al.*, 1997a), accompanied by commentaries (Erickson, 1997; Keller, 1997). These three papers mark the beginning of an exciting period of single titin molecule stretching efforts and a number of significant results have followed (Carrion-Vazquez *et al.*, 1999a; Carrion-Vazquez *et al.*, 1999b; Kellermayer *et al.*, 1998; Marszalek *et al.*, 1999; Oberhauser *et al.*, 1999; Oberhauser *et al.*, 1998; Rief *et al.*, 1998). Additional results have also been reported in recent scientific meetings and are rapidly forthcoming. Reviews on these single molecule studies are appearing (e.g. Kellermayer, *et al.*, 2000).

In the first full-length publication, Tskhovrebova and coworkers (Tskhovrebova *et al.*, 1997) performed mechanical experiments on single molecules of titin to determine their

viscoelastic properties using the LOT technique. They found that titin is elastic on a fast (0.1s) time scale and the force-extension data can be fitted with random-coil polymer models having two different segments of entropic springs. One segment was attributed to the entropy of straightening folded Ig and Fn3 modules of titin; the other was attributed to the extension of the polypeptide chain in the PEVK region. Both FJC and WLC models (see Section 2 for model details) fitted the data similarly well with L_K (segment length) $\cong 2L_P$ (persistence length) $\cong 0.35$ nm for the PEVK region and the over 10-fold greater elastic parameters for the string of folded Ig/Fn3 domains (Fig. 8A). On a slower time scale of seconds and above a certain force threshold of a few tens to hundreds of pN, the stretched titin molecule displayed stress-relaxation in rapid steps of 3-10 pN. This drop of tension was correlated to an increase of the entropic chain length of 19 ± 11 nm from yielding of internal structures, probably the unfolding of Ig and Fn3 domains (Fig. 8B). It is clear that the observed unfolding relaxation behavior deserves further quantification.

Kellermayer and coworkers (Kellermayer *et al.*, 1997) performed similar LOT measurements of the force required to stretch a single titin and similarly revealed that titin behaves as a highly nonlinear entropic spring. The transition from a rapid to a more gradual tension increase around 20 to 30 pN per titin molecule was attributed to Ig and Fn3 domain unfolding. Refolding in a low-force transition below 2.5 pN was also observed. The authors fitted their initial tension *vs.* extension data and the force release data to entropic spring models, and observed that a persistence length of 2.0 nm most likely describes single denatured titin behavior. Only one-segment WLC fits were performed. The stretch-relaxation force hysteresis was attributed to a difference between the unfolding and refolding kinetics of titin folded domains. The authors also concluded that scaling the molecular data up to sarcomeric dimensions reproduced many features of the passive force *vs.* extension curve of muscle fibers. Although it was noted that a fraction of the molecule (5 to 40 percent) remained permanently unfolded, the authors did not resolve the two sequential WLCs (c.f. Tskhovrebova *et al.* (1997)). In their LOT setup apparently one to three T1 titins were stretched at a time.

Rief and coworkers (Rief *et al.*, 1997a) used atomic force microscopy (AFM) to investigate the mechanical properties of titin. Individual titin molecules were repeatedly stretched between a gold substrate and an AFM tip, and the force-extension behavior was recorded and analyzed. At large extensions, the restoring force exhibited a striking sawtooth-like pattern between 150 pN to 300 pN, with a periodicity that varied between 25 and 28 nanometers (see Fig. 8D). They proposed that these sawtooth-like patterns arose from the unfolding of titin

Ig domains. They confirmed this by stretching engineered recombinant titin Ig segments of two different lengths and observed the same pattern. The unfolding forces increased linearly from 150 to 300 pN when pulling speed was varied exponentially from 0.01 μm/s to over 10 μm/s. Upon relaxation, refolding of Ig domains was observed and repeat stretching was demonstrated.

Kellermayer and coworkers (Kellermayer *et al.*, 1998) extended their single-molecule mechanical works to focus on Ig and Fn3 complete unfolding at high forces (Fig. 8C). The force exerted on single titin molecules by the LOT was claimed to be above 400 pN. The high external forces resulted in complete mechanical unfolding of the molecule, characterized by the disappearance of force hysteresis at high forces. This also allowed WLC fitting to the unfolded chain to a greater chain length. Titin refolded following complete denaturation, as the hysteresis at low forces reappeared in subsequent stretch-release cycles. The broad force range of the unfolding force was attributed to variations between Ig and Fn3 modules in the native titin having different activation energies for their unfolding. However, the LOT force calibration in this work is complicated (see Section 2).

Rief and coworkers (Rief *et al.*, 1998) also followed up their AFM work on titin and compared the unfolding forces of defined regions of different titin isoforms. Constructs comprising six to eight Ig domains located in the mechanically active I-band segment of titin were compared to those containing Fn3 and Ig domains from the A-band part. They improved the spatial resolution of their AFM to detect differences in length as low as a few amino acids per titin folded domain. The authors showed that the unfolding forces ranged between 150 and 300 pN and differed systematically between the constructs. Fn3 domains in titin exhibited 20% lower unfolding forces than Ig domains and Fn3 domains from tenascin unfolded at forces only half those of titin Fn3 domains (see below). The authors suggest that the tightly folded titin domains are designed to maintain their structural integrity and, hence, unfolding is unlikely under physiological sarcomere forces.

Oberhauser and coworkers (Oberhauser *et al.*, 1998) also studied the extracellular matrix protein tenascin using AFM techniques and compared the results with titin. They found that tenascin, which has many Fn3 modules, is also an elastic protein and could be stretched to several times its resting length. The investigation closely paralleled the earlier AFM studies on titin unfolding. Force-extension curves showed a sawtooth pattern, with peaks of force around 100 pN that depended linearly on log (pulling speed). The leading edges of the force peaks were well fitted by WLC models with $L_p \cong 0.4$ nm and each was approximately 25 nm apart in the chain contour length. The authors found similar stretch-induced unfolding of its Fn3 domains in

recombinant tenascin fragments encompassing the 15 Fn3 domains of tenascin. Refolding of tenascin after stretching was observed when the force was reduced to near zero and showed a double-exponential recovery with time constants of 42 domains refolded per second and 0.5 domains per second.

In yet another extension of the AFM work on titin, Carrion-Vazquez and coworkers (Carrion-Vazquez *et al.*, 1999a) demonstrated that AFM techniques could detect contour length changes due to the insertion of a few amino acids in an Ig domain. The authors amplified the mechanical features of a single domain by engineering polyproteins composed of up to 12 identical repeats. They then showed that upon mechanical unfolding, mutant polyproteins containing five extra glycine residues extended 2.0 nm per module farther than the wild-type polyproteins. When similar insertions were near the N or C termini, the 4 nm per amino acid increase did not show up in the unfolding sawtooth pattern.

In a more comprehensive report, Carrion-Vazquez and coworkers (Carrion-Vazquez *et al.*, 1999b) also investigated the detailed folding/unfolding pathway of a titin Ig module using AFM and found insightful correspondence with chemical induced folding/unfolding pathway. By engineering a protein made of tandem repeats of identical Ig modules, the authors were able to get explicit pulling-rate dependent data on the unfolding rate of a single protein domain that can be accurately extrapolated to zero force. When this was compared with chemical unfolding rates for untethered modules extrapolated to 0 M denaturant, the two results were in good agreement. Their evidence also supported that the transition state for unfolding appears at the same position in terms of the reaction coordinate on the folding pathway when assessed by either the AFM force or chemical stress.

In the next work, Marszalek and coworkers (Marszalek *et al.*, 1999) resolved a mechanical unfolding intermediate in a titin Ig domain, and supported this finding with careful computer simulations and mutation investigations. Applying AFM extension to a string of multiple copies of one Ig domain, the authors found an abrupt extension of each domain by about 0.7 nm before the first unfolding event. This fast initial extension before a full unfolding event was thought to produce a reversible unfolding intermediate that is about 15% longer. Steered molecular dynamics simulations on the unfolding of the same Ig module showed that a pair of hydrogen bonds near the amino terminus of the domain may rupture first under force extension and cause an extension of about 0.6 nm, in good agreement with the AFM number of 0.7 nm. Furthermore, it was shown that disruption of these hydrogen bonds by site-directed mutagenesis eliminated the unfolding intermediate. It was noted that the existence of this unfolding

intermediate might also extend titin domains up to 15% of their slack length and contribute to titin elasticity in sarcomere.

In the latest report of their series of AFM observations on titin constructs, Oberhauser and coworkers (Oberhauser *et al.*, 1999) demonstrated that, after repeated mechanical extension/relaxation cycles, tandem modular proteins can misfold into a structure formed by two neighboring modules. The misfolding altered the mechanical topology of the modules and was shown to be fully reversible and about as stable as the original fold. This showed that if titin domains unfold under sarcomere stress, it could refold into unusual conformations. The work demonstrated further that AFM has the power to capture, in real time, rare misfolding events at the level of a single protein.

3.2. Comparison of AFM and LOT Unfolding Data

The data on titin stretching obtained from the AFM and LOT at first glance appear quantitatively and qualitatively different, especially the absolute force at which titin domains unfold and the lack of sawteeth in the LOT studies from Kellermayer *et al.* (1997). Many factors may contribute to these discrepancies. The difference in instrumentation design, force calibration, protein attachment, geometry of stretching and data acquisition has been discussed above. The large force and loading rate of AFM and the lower force and slower loading rate of LOT are also major factors here.

One possibility arises from the fact that AFM was performed on a film of titin or titin fragments adsorbed onto a substrate. It is conceivable that the protein adheres to the substrate at multiple points and, upon stretch, the protein-substrate interaction ruptures sequentially, without unfolding of domains. Several facts argue against the sequential desorption of the protein from the surface. The rupture forces seen for native titin and titin fragments are widely dispersed, whereas those for the I27 homopolymer form a tight distribution which can be fit by the bond lifetime model (Fig. 4D). The increase of contour length following one of the ruptures is exactly what one would expect for a protein domain with 89 amino acids. Each domain would have to adhere to the surface at the same position to exhibit this behavior and still have the ruptures result from surface interactions rather than domain unfolding. The best evidence for domain unfolding comes from the study by Carrion-Vazquez *et al.* (1999a) where five glycine residues were inserted into the core of the immunoglobulin domain. Upon extending this polyprotein with the AFM, they found that the increase in the contour length is what would be expected for the addition of the five amino acids to the sequence. Adhesion to the substrate cannot explain this

difference between the wild-type I27 domain and that with an insert in the core of the domain. These results argue strongly that the sawtooth pattern results from domain unfolding and not rupture of protein-substrate adhesion.

The apparent lack of the saw-tooth pattern in LOT is likely due to the several reasons. First, the loading rates on titin are significantly different. Kellermayer *et al.* (1997) stretched the titin at a constant rate from 1-6 pN/s (90 nm/s) until a maximum force was reached and then the polymer was relaxed. This loading rate is much less than that of AFM measurements and unfolding dynamics of the titin domain can be significantly different (See Section 2.1). Second, the AFM cantilever is much stiffer than LOT trap. The stretch-induced unfolding of each titin domain should increase the contour length by an amount of about 25 nm. In AFM, the stiff cantilever recoils very little and the force (which depends sharply on the ratio of the end-to-end distance to the contour length) is reduced greatly. The force has to increase gradually to cause another domain to unfold, leading to a regular saw-tooth pattern. In LOT, the softer trap stiffness means the large backward movement of the bead causes the end-to-end distance of the titin segment to also increase, so the force on the molecule drops only slightly after a domain unfolding event. This contributes to the absence of any clear saw-tooth pattern in LOT experiments even as domains unfold (Kellermayer *et al.* 1997; Tskhovrebova *et al.*, 1997; Kellermayer, *et al.*, 2000).

Kellermayer *et al.* (1998, 1997) observed a striking hysteresis by comparing the extension and relaxation curves for native titin. The extension curve followed the response of the WLC model up to about 20 pN whereupon a "stretch transition" occurred, which results in less elastic force for a given extension. Kellermayer and colleagues have suggested that this transition may be a structural change. Evans and Ritchie (1999) showed that this change in the slope of the F *vs.* d curve could be attributed to the steady unfolding of domains connected by a flexible linker. The low force loading of LOT at *ca.* 13 pN/s results in the domains unfolding at a much lower force without the sawtooth discontinuities seen in the AFM experiments. In the extension portion of the curve, the low force data was fit with the WLC model with a persistence length of 4Å and a contour length of 2.2 μm. The release curve of the same segment fits the WLC model with a persistence length of 9 Å and a contour length of 3.0 μm. The hysteresis was caused by the mechanical unfolding of the Ig and Fn3 domains in titin. After the stretched titin was allowed to relax, the domains refolded and upon restretching the hysteresis curve was recovered.

Tskhovrebova *et al.* (1997) used two different methods to extend titin. For the dynamic extension of native titin, the bead was held in the optical trap and the stage was driven with a

triangle wave with a frequency of 2 Hz. The amplitude of the stage motion was *ca.* 4 μm peak to peak, with a maximum force of about 70 pN. The extension/retraction rates were held constant, however, the loading force increased nearly exponentially. The maximal loading rate was of the order of 1 nN/s. For the static extension method, titin was stretched in steps of about 250 nm and then held at each stage until the stress relaxation was complete on the order of seconds. The force jumped to over 120 pN after each step extension. The effective loading rate was much higher than that in the dynamic extension case, favoring domain unfolding during the waiting periods, rather than during the stretching periods. The dynamic force-extension of native titin yielded a curve that could be readily fit by the WLC model. In Fig. 8A, the solid line is the data and the dots represent the fit to a single component WLC, with a persistence length of 0.76 nm and a contour length of 1932 nm. The open circles are for a two component WLC model, with persistence lengths of 4.15 and 0.19 nm and contour lengths of 1174 and 791 nm respectively. The dynamic extension was accomplished by moving the stage at a rate of 16 μm/s. At this rapid rate of extension and low force, the Ig and Fn3 domains will not unfold and all of the extension was attributed to the straightening of the molecule and the extension of the PEVK segment.

The static extension of native titin by Tskhovrebova *et al.* (1997) (Fig. 8B), in contrast, shows the unfolding of domains. The titin was stretched by 250 nm and then was held at that position until the stress-relaxation was complete. As is clearly seen in Fig. 8B, the force increases rapidly upon the initial stretch and then the force decreases in a stepwise manner, with an average step of 20 nm. The steps are less than the fully extended length of 38 nm for 100-residue domains, because the forces are not great enough to fully extend the molecule. This stepwise reduction in force when titin is stretched and held at a certain length was modeled by Rief *et al.* (1998) using the lifetime and unfolding reaction width determined from their AFM experiments. Their Monte Carlo simulation of the static extension of titin yields the same stepwise unfolding behavior seen experimentally with the optical trap system.

3.3. Molecular elasticity results

The different results obtained for the different methods of extension with optical traps and AFM exemplify the importance of the loading rate or time that the load is applied to the polymer in determining the outcome of single molecule mechanics. While much of these differences are attributable to Ig and Fn3 domain unfolding/refolding, the PEVK and other titin motifs must also contribute to the overall molecular elasticity. As described in Section 2.2, several models have

been used for chain molecule extension behavior and are approximations at various levels of simplifications. Clear limitations of these models include the lack of direct loading rate and history-dependence of the extension force. Nevertheless, these models have offered useful parameters for comparing molecular elasticity of titin motifs.

Single molecule measurements generally favor the use of the WLC model as the basis for parameterizing the full range of titin elasticity. The results suggest that the elasticity of whole molecule titin results from the extension of two components: a stiff entropic spring for titin motifs including PEVK, N2-A and N2-B unique insertions and the unfolded peptides from the Ig and Fn3 modules, and a soft entropic spring consisting of folded beads of Ig and Fn3 domains (Fig. 3 and Freiburg *et al.*, 2000). The persistence lengths deduced from the single titin measurements are summarized in Table 4. The stiff entropic string has a reported persistence length range of 0.15-0.8 nm (Jin *et al.*, 2000; Kellermayer *et al.*, 1998; Kellermayer *et al.*, 1997; Rief *et al.*, 1997a; Tskhovrebova *et al.*, 1997). The soft entropic spring has a corresponding persistence length range of 4.6-15 nm (Higuchi *et al.*, 1993; Kellermayer *et al.*, 1997; Tskhovrebova *et al.*, 1997). The whole titin acts as a serial spring and lengthens first its soft spring under low force of less about 5 pN/titin and then its stiff spring under high force of larger about 5 pN.

Tskhovrebova *et al.* (1997) made an effort to characterize both the soft and stiff springs by two segment fits to the LOT force-extension data. Most other studies did not attempt to extract beyond single segment fits (Higuchi *et al.*, 1993; Kellermayer *et al.*, 1998; Kellermayer *et al.*, 1997; Rief *et al.*, 1997a). Furthermore, the persistence parameter for each titin motif appears to be dependent significantly on solution ionic conditions (Jin *et al.*, 2000), which are different for each research group (Table 4). Nevertheless, it is a consensus that the soft spring segment, with persistence length of the order of its 4 nm-long Ig and Fn3 domains, is about 10 times more compliant than that of the stiff spring segment, with the persistence length of the order of the 0.38nm peptide bond. Additional support for such a broad distribution of stiffness within titin also comes from recent immunoelectron microscopy studies (Freiburg *et al.*, 2000; Granzier *et al.*, 1996; Linke *et al.*, 1998; Linke *et al.*, 1996; Linke *et al.*, 1999; Trombitas *et al.*, 1998), using site-specific antibody markers to resolve details of the extension of various titin motifs (Freiburg *et al.*, 2000). However, a fuller discussion of these non-single titin results is beyond the scope of this review.

4. Dynamic force spectroscopy and mechanical unfolding/folding

The forced unfolding of Fn3 and Ig domains has provided valuable insight into how titin domains might behave under more stressful conditions *in vivo*. Additionally, these experiments have provided new information on how proteins respond to mechanical stress. The power of dynamic force spectroscopy in revealing subtle behavioral changes in protein folding is illustrated by the work of Oberhauser *et al.* (1999) who demonstrated that the Ig modules in a homopolymer of I27 can misfold to a dimeric form after a few mechanical unfolding-refolding cycles. This approach opens the door to investigate the means of reversing undesirable misfolding of proteins, a topic of major physiological and biotechnology interests. It also demonstrates the efficiency of refolding of titin domains after repeated mechanical unfolding. Many eukaryotic proteins have evolved as modular constructs that must fold co-translationally, which is facilitated by chaperonins (Netzer and Hartl, 1997). In prokaryotes, proteins are believed to fold post-translationally, which may explain, in part, why many modular proteins are not expressed well or appear as inclusion bodies of misfolded proteins in *E. coli*. However, if a protein misfolds, intracellular repair mechanisms will correct the misfolding, e.g. GroEL/GroES allows *E. coli* proteins to refold by first unfolding them (Shtilerman *et al.*, 1999). It is conceivable that both mechanical and chemical unfolding of proteins may be an integral part of the cellular repair mechanisms of misfolded proteins.

Repeated extension and relaxation of native titin results in the loss of the sawtooth pattern and the hysteresis in the force-distance curves. One possible cause may be the slow and rate limiting proline *cis-trans* isomerization as first postulated by Kellermayer *et al.* (1997). Recent studies by Plaxco *et al.* (1997) showed that two Fn3 domains, with similar, characteristic beta folds and 30% sequence identity, had refolding rates different by two orders of magnitude. The folding of the slow folding module was limited by proline isomerization, which can be catalyzed by the addition of prolyl peptidyl *cis-trans* isomerase (PPI), giving a three-fold reduction in the folding time. If the repeated extension of native titin results in an increase in the amount of *cis*-proline isomers, this could account for the effects observed during the repeated mechanical unfolding of the protein. However, other mechanisms that can lead to a kinetic folding trap cannot be discounted. The possibility that prolyl isomerase or chaperonins are involved in accelerating titin folding in solution and *in situ* is well worth exploring.

The folded lifetime at zero force and the width of the unfolding potential (or length along the reaction coordinate, see Fig. 4A) are the two defining parameters of how the protein will

respond to load. Rief *et al.* (1998) showed that for native titin, $\tau_0 = 30{,}000 \pm 10{,}000$ s and $x_u = 0.3 \pm 0.1$ nm based on the average unfolding force at different speeds. However, for human tenascin Fn3 domains, $x_u = 0.55 \pm 0.1$ nm, which indicates that tenascin Fn3 domains are more sensitive to applied unfolding forces than is native titin. From the I27 polyprotein, Carrion-Vazquez *et al.* (1999b) were able to demonstrate that the I27 Ig domain was even more stable to applied forces with $\tau_0 = 3{,}000$ s and $x_u = 0.25$ nm. One can infer that the domains of titin have evolved to be stable to high forces when they are applied for a short period of time. Any applied force will bias a protein to unfold if it is applied for a long enough time. If a protein is stable to high forces applied over a short period of time, it follows from Eqn. 2 that it will also be more stable to small forces applied over a longer period of time. This results from the shorter reaction width and the concomitant lower reduction in lifetime for any given force applied to the protein.

The notion of mechanical unfolding of proteins has captured the imagination of the protein folding community, which has given rise to several theoretical analyses of forced unfolding of proteins (Gao *et al.*, 2000; Klimov and Thirumalai, 1999; Klimov and Thirumalai, 2000; Krammer *et al.*, 1999; Lu *et al.*, 1998; Lu and Schulten, 1999a; Lu and Schulten, 1999b; Lu and Schulten, 2000; Paci and Karplus, 1999; Paci and Karplus, 2000; Rohs *et al.*, 1999; Socci *et al.*, 1999; Zhang *et al.*, 1999). The thorough understanding of two-state folding proteins (proteins which have no intermediates between the folded and unfolded states) is crucial for understanding how proteins with more complex folding processes fold in cells (Eaton *et al.*, 2000; Levitt *et al.*, 1997; Onuchic *et al.*, 1997). Because many load-bearing protein structures are aggregate systems, a thorough understanding of how individual protein molecules respond to force will provide fundamental insights into how supramolecular assemblies perform their functions in cells and tissues.

Since β-barrels are fundamental and major folding motifs in nature, the mechanical unfolding of titin Ig domains are likely of general significance and application. It is therefore worthwhile to summarize the current state of knowledge of the unfolding properties of the titin Ig, Fn3 and tenascin domains as characterized by AFM. An important observation was that the average unfolding force for the modules of native titin was dependent upon the log of the extension speed (Rief *et al.*, 1997a). While this behavior was predicted by Evans and Ritchie (1997), the results from Rief and colleagues represent the first experimental evidence for the predicted speed dependence of forced rupture of biomolecular interactions (Rief *et al.*, 1998). Comparison of the speed dependence of native titin with that of a recombinant tenascin fragment (primarily Fn3 domains) demonstrates the importance of the loading rate in the characterization

of the mechanical properties of a protein. The tenascin domains have a folded lifetime similar to that of the domains in titin. However, the unfolding reaction width was larger than the average width of the titin domains. This increased width leads to a lower slope in the plot of rupture force *vs.* log (extension rate). This decreased sensitivity to the loading rate implies that tenascin cannot withstand rapid extensions as well as titin. By using recombinant fragments of different parts of skeletal titin, Rief *et al.* (1998) showed that these different domains have different average rupture forces, even though the rupture of individual domains ranged between 150-300 pN. Whether this heterogeneity in rupture forces plays a physiological role or is merely the consequence of different amino acid sequences needed for the protein to fulfill its other roles is yet to be determined. At this point it would be pure speculation as to whether these differences in the stability of the titin domains to applied force has evolved to fulfill some function or simply adventitious.

These early experiments on native proteins and fragments of the proteins suggested that the AFM could be a powerful tool for studying protein folding. However, the heterogeneity of the native titin and the recombinant fragments makes a detailed analysis a difficult task. Carrion-Vazquez *et al.* (1999b) have made a "cleaner" system for studying the forced unfolding properties of titin Ig domains by preparing a homopolymer of Ig domains. Recombinant methods were used to prepare the polymer with twelve identical domains of module 27 from the I-band of human cardiac titin. With a polymer of identical Ig domains, any variation in the unfolding properties is due to random processes and not to differences in the intrinsic properties of the domain. This is demonstrated well by the histogram of unfolding forces for an octamer of the I27 domain (Fig. 4D). The histogram of the unfolding forces of the eight I27 domains can be fit readily by a Monte Carlo simulation of the mean unfolding forces with an unfolding distance of 0.25 nm, a folded lifetime of 3000 s and a pulling rate of 0.6 nm/ms. This folded lifetime is an order of magnitude shorter than that determined by Rief *et al.* (1998) for native titin. The identical domains of the recombinant homopolymers allow experimentally determined parameters to be assigned as properties of the domains. This ability has allowed Carrion-Vazquez *et al.* (1999b) to compare directly chemical unfolding of isolated I27 domains with the force unfolding of polymers of the same domain. Extrapolating the chemical unfolding data to a zero concentration of guanidinium hydrochloride gives a folded lifetime of 2000 s and a folding rate of 32 s^{-1}. Forced unfolding of the polymer of I27 gives a folded lifetime of 3000 s and a folding rate of 1.2 s^{-1}. The kinetic rates for unfolding and folding can be used to estimate the activation free energy of unfolding and folding. The activation free energy for unfolding the I27

domain was found to be 22.0 kcal/mol for chemical unfolding and 22.2 kcal/mol for forced unfolding. The activation free energy for folding of I27 was found to be 15.4 kcal/mol for chemically unfolded protein and 17.3 kcal/mol for force unfolded protein. The barrier heights to unfolding by the two methods are almost identical, which suggests that the unfolding pathways are similar. The barriers to refolding by the two methods are significantly different. The 1.9 kcal/mol difference can be attributed to the entropic cost of tethering. As was discussed above, even a small force applied to a polypeptide chain will greatly decrease the folded lifetime. The extension of the protein decreases the conformational entropy of the polypeptide chain, which will slow down the refolding process. The similarity of the reaction coordinates between chemical and forced unfolding is at first surprising. However, considering the β-barrel structure of the Ig domains and the fact that the amino and carboxy termini are about 180° apart this seems quite reasonable. There are now both computational and experimental evidence that the first step of unfolding of the Ig domains is the rupture of hydrogen bonds between the A and B β-strands (Marszalek *et al.*, 1999). The rupturing of these hydrogen bonds leads to a 6.6 Å extension of the Ig domain at a force of about 100 pN. Molecular dynamics modeling of the extension of Ig domains indicates that the next step is the rupture of the patch of hydrogen bonds between the A′ and G β-strands (Lu *et al.*, 1998) followed by the extension of the polypeptide. The effect of chemical denaturants on protein structure is to both weaken hydrogen bonds and weaken hydrophobic interactions. The folding of small, single domain proteins arises largely from the cooperative formation of hydrogen bonds. If strain placed on hydrogen bonds causes them to first weaken and then rupture, a sequence similar to that induced by chemical denaturants, then the unfolding pathways taken by the two unfolding methods would be expected to be similar. However, a small change in protein conformation could have dramatic effects upon the forced unfolding pathway, while the chemical unfolding pathway could remain the same. If the amino and carboxy termini are closer together, then the forced unfolding pathway will be very different from what it is for the Ig domain with the termini opposite from one another (Klimov and Thirumalai, 1999). It very well may be that the Ig domain is a special case where the unfolding pathways are similar for chemical and forced unfolding.

While other arrangements of the termini of the domains forming a large polyprotein such as titin are possible, having them 180º apart is clearly an advantage for a protein designed to sustain a force along its length. If the termini were close to one another, the strain would not be distributed throughout the molecule as it is with the Ig domains. This could lead to sequential unfolding of the secondary structural folds rather than the two-state unfolding observed with the

Ig domains. While a polymer of T4 lysozyme has been studied, it was not stretched between its termini and Yang *et al.* (2000) did not investigate the kinetics of the folding and unfolding.

5. Summary and discussion

5.1. Elasticity: From single molecules to tissues

Mechanically, titin is a modular polymer that acts as a multistage spring that adjusts both its length and its apparent extension stiffness in response to axial stress. Without external force, the necklace of beads acts as an entropic spring. Each folded domain, by its characteristic folding and idiosyncratic resistance to stretch, acts as a latent spring. Under external force, each domain "yields" and unfolds at a threshold values of force and loading rate. The disordered polypeptides are then "drafted" to participate in the entropic elasticity of the newly adjusted spring that now has a longer contour length and a different spring constant. Upon relaxation, the "draftees" fold individually and are "discharged" in an order that is determined by the rate and pathway of folding. Titin therefore undergoes the same "yield" phenomenon as the sarcomere and, indeed, as any composite biological material.

The behavior of this multistage spring therefore bears striking resemblance to the segmental extension of the sarcomere subjected to stretch. In the sarcomere, the tension rises mildly first and then exponentially until the threshold value at the yield point, where it levels off or drops. The force rise can be resolved into two mechanical phases by plotting log tension *vs.* sarcomere length (Wang, *et al.*, 1991, 1993), or three phases by plotting stiffness *vs.* tension (Granzier and Wang, 1993a; Granzier and Wang, 1993b). Each mechanical phase varies with the type of titin isoforms expressed in the muscle. It is conceivable that these mechanical phases correspond structurally to the straightening of Ig domains and the extension of PEVK or even the rupture of interfilament interactions between actin-nebulin co-filaments and myosin thick filaments. However, the major yield point of the sarcomere is controlled by the strength of interaction of titin with the thick filaments (Wang *et al.*, 1991, 1993). Such "external force" imposed by thick filaments on titin may prevent the unfolding of Ig and Fn3 domains in the A band region of titin.

The fact that Ig and Fn3 modules do not unfold/refold significantly during physiological cycles is important, because it preserves the efficiency of striated muscles, as the extension/relaxation hysteresis is kept to a minimum. The unfolding of domains provides a large reserve of titin chain length and can act as a safety mechanism against sarcomere damage or

fracturing under extreme pathological extension. The refolding ability provides a pathway to regenerate the original multistage elastic structure titin.

5.2. Emerging Trends

We can expect more concerted efforts in detailed examination of other titin motifs using a new generation of single molecule research tools and new techniques of expressing engineered domains and polyproteins. Recently, we have undertaken an AFM study of the elasticity of a 52KDa PEVK motif of human fetal skeletal muscle titin (Jin *et al.*, 2000). The worm-like chain (WLC) models adequately describe its force-extension curves. The persistence length varies with Ca^{2+} concentration and ionic strength, suggesting that elasticity may be modulated by ionic conditions in muscle. Other constructs of specific titin regions are sure to follow.

The molecular insights reviewed here were made possible by single molecule techniques that are evolving constantly and rapidly. In biological AFM, current advances include the wider adaptation of the acoustic and magnetic tapping modes used under physiological conditions, development of faster AFM, smaller cantilevers (Viani *et al.*, 1999a; Viani *et al.*, 1999b), functionalized nanotubes (Cheung *et al.*, 2000; Nagao *et al.*, 2000; Woolley *et al.*, 2000), better characterization of substrate effects (Forbes, 2001; Glazier *et al.*, 2000; Rao *et al.*, 1997), continued advance in high resolution cryo-AFM (Czajkowsky and Shao, 1998; Shao *et al.*, 1996; Shao *et al.*, 1995) and instrumentation for force/volume/quantitative phase/other modes of data acquisition (see, e.g., another chapter in this series, (Zlatanova *et al.*, 2000)). LOT technology has also been improved with better calibration methods (Bennink *et al.*, 1999; Wang *et al.*, 1997b), force-feedback modes (Wang *et al.*, 1998; Wang *et al.*, 1997b), multiple optical traps (Svoboda and Block, 1994; Visscher and Block, 1998; Visscher, *et al.*, 1996), high-force setups (Kellermayer *et al.*, 1998), and reduced sample heating and damage (Kuo, 1998; Neuman, *et al.*, 1999). For both LOT and AFM, more systematic considerations of the thermal noise behaviour and filtering may improve the measurement signal-to-noise ratio.

Other techniques for force measurements in biological systems, including membrane micropipette aspiration/bioforce transducer (Evans *et al.*, 1995) and the more traditional surface force apparatus (Helm *et al.*, 1991), are also being improved to compliment these two core single molecule techniques, AFM and LOT (see, e.g., review by Leckband, (2000)). Methods that allow simultaneous measurements, e.g. AFM and fluorescence, and the application of energy transfer to study protein folding/unfolding at the single molecule level, are likely to provide the

next quantum leap in our pursuit of single molecule mechanics and single molecule biology (Fernandez *et al.*, 2001; Mehta *et al.*, 1999; Weiss, 1999; Zhuang *et al.*, 2000).

Note added in proof

Recent structural and mechanical studies of the PEVK segment shed new light upon the structural basis of elasticity in this region of titin. Previously, the PEVK region of titin was assumed to be made up of random coils or unfolded polymer as in the mechanical analysis discussed above. New studies have now shown that the PEVK segment is modular and contains tandem repeats of modules containing 28 amino acids (Freiburg *et al.*, 2000; Greaser, 2001; Gutierrez-Cruz *et al.*, 2001). The existence of folded structure, in the form of polyproline-II helices (PPII), is demonstrated by NMR and circular dichroism of synthetic peptides and cloned PEVK protein (Ma *et al.*, 2001). Measurement of the molecular elasticity of cloned PEVK domain using AFM force spectroscopy is found to contain both entropic and enthalpic contributions, and its elasticity is sensitive to the total ionic strength of the environment (Jin *et al.*, 2001). These direct measurements corroborate the deduced behavior of PEVK from mechanical measurements of single myofibrils as studied by Linke and colleagues (Linke, 2000; Linke *et al.*, 1998; Minajeva *et al.*, 2001).

The elasticity and organizational roles of titin have also found relevance in tissues other than striated sarcomeres. Recent titin localization and mechanical studies of chromosomes clearly indicate important roles for titin in chromosome structure and mechanics (Machado and Andrew, 2000). The reported presence of smooth muscle titin, and its organizational roles in myosin assembly, raises the possibility that titin may yet be a new class of elastic cytoskeletal molecules that are widespread in muscle as well as nonmuscle cells (Keller *et al.*, 2000). Defects in titin have now been linked to several types of muscular dystrophy (Haravuori *et al.*, 2001; Sorimachi *et al.*, 2000; van der Ven *et al.*, 2000).

Acknowledgements

We thank Dr. M. Kellermayer and the other two expert referees for their insightful comments on the original version of this review and detailed suggestions, which we have gratefully adopted. We are also grateful for the helpful comments from Dr. Mike Lewis and other members of the Wang research group.

References

Ashkin, A. (1980) Applications of laser-radiation pressure. *Science* **210,** 1081-1088.

Ashkin, A. (1992) Forces of a single-beam gradient laser trap on a dielectric sphere in the ray optics regime. *Biophys. J.* **61,** 569-582.

Ashkin, A., Dziedzic, J. M., Bjorkholm, J. E. and Chu, S. (1986) Observation of a single-beam gradient force optical trap for dielectric particles. *Opt. Lett.* **11,** 288-290.

Bell, G. I. (1978) Models for the specific adhesion of cells to cells. *Science* **200,** 618-627.

Bennink, M. L., Scharer, O. D., Kanaar, R., Sakata-Sogawa, K., Schins, J. M., Kanger, J. S., de Grooth, B. G. and Greve, J. (1999) Single-molecule manipulation of double-stranded DNA using optical tweezers: Interaction studies of DNA with reca and yoyo-1. *Cytometry* **36,** 200-208.

Binnig, G., Quate, C. F. and Gerber, C. (1986) Atomic force microscope. *Phys. Rev. Lett.* **56,** 930-933.

Block, S. M. (1992) Making light work with optical tweezers. *Nature* **360,** 493-495.

Block, S. M. (1995) Nanometers and piconewtons - the macromolecular mechanics of kinesin. *Trends Cell Biol.* **5,** 169-175.

Bouchiat, C., Wang, M. D., Allemand, J. F., Strick, T., Block, S. M. and Croquette, V. (1999) Estimating the persistence length of a worm-like chain molecule from force-extension measurements. *Biophys. J.* **76,** 409-413.

Butt, H. J. and Jaschke, M. (1995) Calculation of thermal noise in atomic-force microscopy. *Nanotechnology* **6,** 1-7.

Carrion-Vazquez, M., Marszalek, P. E., Oberhauser, A. F. and Fernandez, J. M. (1999a) Atomic force microscopy captures length phenotypes in single proteins. *Proc. Natl. Acad. Sci. U. S. A.* **96,** 11288-11292.

Carrion-Vazquez, M., Oberhauser, A. F., Fowler, S. B., Marszalek, P. E., Broedel, S. E., Clarke, J. and Fernandez, J. M. (1999b) Mechanical and chemical unfolding of a single protein: A comparison. *Proc. Natl. Acad. Sci. U. S. A.* **96,** 3694-3699.

Cheung, C. L., Hafner, J. H. and Lieber, C. M. (2000) Carbon nanotube atomic force microscopy tips: Direct growth by chemical vapor deposition and application to high-resolution imaging. *Proc. Natl. Acad. Sci. U. S. A.* **97,** 3809-3813.

Chilkoti, A., Boland, T., Ratner, B. D. and Stayton, P. S. (1995) The relationship between ligand-binding thermodynamics and protein-ligand interaction forces measured by atomic force microscopy. *Biophys. J.* **69,** 2125-2130.

Chu, V., Freitag, S., Le Trong, I., Stenkamp, R. E. and Stayton, P. S. (1998) Thermodynamic and structural consequences of flexible loop deletion by circular permutation in the streptavidin-biotin system. *Protein Sci.* **7,** 848-859.

Cleveland, J. P., Manne, S., Bocek, D. and Hansma, P. K. (1993) A nondestructive method for determining the spring constant of cantilevers for scanning force microscopy. *Rev. Sci. Instrum.* **64,** 403-405.

Czajkowsky, D. M. and Shao, Z. F. (1998) Submolecular resolution of single macromolecules with atomic force microscopy. *FEBS Lett.* **430,** 51-54.

Dai, J. W. and Sheetz, M. P. (1998) Cell membrane mechanics. In *Methods in cell biology, Vol. 55*, (ed. M. P. Sheetz), pp. 157-171, Academic Press, San Diego.

Derose, J. A., Thundat, T., Nagahara, L. A. and Lindsay, S. M. (1991) Gold grown epitaxially on mica - conditions for large area flat faces. *Surf. Sci.* **256,** 102-108.

Eaton, W. A., Munoz, V., Hagen, S. J., Jas, G. S., Lapidus, L. J., Henry, E. R. and Hofrichter, J. (2000) Fast kinetics and mechanisms in protein folding. *Annu. Rev. Biophys. Biomolec. Struct.* **29,** 327-359.

Erickson, H. P. (1997) Protein biophysics - stretching single protein molecules: Titin is a weird spring. *Science* **276,** 1090-1092.

Evans, E. (1998) Energy landscapes of biomolecular adhesion and receptor anchoring at interfaces explored with dynamic force spectroscopy. *Faraday Discuss.* **111,** 1-16.

Evans, E. (1999) Looking inside molecular bonds at biological interfaces with dynamic force spectroscopy. *Biophys. Chem.* **82,** 83-97.

Evans, E. and Ritchie, K. (1997) Dynamic strength of molecular adhesion bonds. *Biophys. J.* **72,** 1541-1555.

Evans, E. and Ritchie, K. (1999) Strength of a weak bond connecting flexible polymer chains. *Biophys. J.* **76,** 2439-2447.

Evans, E., Ritchie, K. and Merkel, R. (1995) Sensitive force technique to probe molecular adhesion and structural linkages at biological interfaces. *Biophys. J.* **68,** 2580-2587.

Fernandez, J. M., Chu, S. and Oberhauser, A. F. (2001) RNA structure - pulling on hair(pins). *Science* **292,** 653-654.

Florin, E. L., Moy, V. T. and Gaub, H. E. (1994) Adhesion forces between individual ligand-receptor pairs. *Science* **264,** 415-417.

Florin, E. L., Rief, M., Lehmann, H., Ludwig, M., Dornmair, C., Moy, V. T. and Gaub, H. E. (1995) Sensing specific molecular-interactions with the atomic-force microscope. *Biosens. Bioelectron.* **10,** 895-901.

Forbes, J. G., Jin, A. J. and Wang, K. (2000) AFM investigation of native nebulin. *Biophys. J.* **78,** 380A.

Forbes, J. G., Jin, A. J., Wang, K. (2001) Atomic force microscope study of the effect of the immobilization substrate on the structure and force-extension curves of a multimeric protein. *Langmuir* **17,** 3067-3075.

Freiburg, A., Trombitas, K., Hell, W., Cazorla, O., Fougerousse, F., Centner, T., Kolmerer, B., Witt, C., Beckmann, J. S., Gregorio, C. C., Granzier, H. and Labeit, S. (2000) Series of exon-skipping events in the elastic spring region of titin as the structural basis for myofibrillar elastic diversity. *Circ. Res.* **86,** 1114-1121.

Funatsu, T., Higuchi, H. and Ishiwata, S. (1990) Elastic filaments in skeletal muscle revealed by selective removal of thin filaments with plasma gelsolin. *J. Cell Biol.* **110,** 53-62.

Furst, D., Osborn, M., Nave, R. and Weber, K. (1988) The organization of titin filaments in the half sarcomere revealed by monoclonal antibodies in immunoelectron microscopy: A map of ten nonrepetitive epitopes starting at the z line extends close to the m line. *J. Cell Biol.* **106,** 1563-1572.

Gao, M., Isralewitz, B., Lu, H. and Schulten, K. (2000) Steered molecular dynamics simulation of the unfolding of multiple titin immunoglobulin domains. *Biophys. J.* **78,** 28A.

Gittes, F. and Schmidt, C. F. (1998) Signals and noise in micromechanical measurements. In *Methods in cell biology, Vol. 55*, (ed. M. P. Sheetz), pp. 129-156.

Glazier, S. A., Vanderah, D. J., Plant, A. L., Bayley, H., Valincius, G. and Kasianowicz, J. J. (2000) Reconstitution of the pore-forming toxin alpha-hemolysin in phospholipid/18-octadecyl-1-thiahexa(ethylene oxide) and phospholipid/n-octadecanethiol supported bilayer membranes. *Langmuir* **16,** 10428-10435.

Grandbois, M., Beyer, M., Rief, M., Clausen-Schaumann, H. and Gaub, H. E. (1999) How strong is a covalent bond? *Science* **283,** 1727-1730.

Granzier, H., Helmes, M., Cazorla, O., McNabb, M., Labeit, D., Wu, Y. M., Yamasaki, R., Redkar, A., Kellermayer, M., Labeit, S. and Trombitas, K. (2000) Mechanical properties of titin isoforms. In *Elastic Filaments of the Cell, Vol. 481*, pp. 283-304.

Granzier, H., Helmes, M. and Trombitas, K. (1996) Nonuniform elasticity of titin in cardiac myocytes: A study using immunoelectron microscopy and cellular mechanics. *Biophys. J.* **70,** 430-442.

Granzier, H. L. and Irving, T. C. (1995) Passive tension in cardiac muscle: Contribution of collagen, titin, microtubules, and intermediate filaments. *Biophys. J.* **68,** 1027-1044.

Granzier, H. L. M. and Wang, K. (1993a) Interplay between passive tension and strong and weak binding cross-bridges in insect indirect flight-muscle - a functional dissection by gelsolin-mediated thin filament removal. *Journal of General Physiology* **101,** 235-270.

Granzier, H. L. M. and Wang, K. (1993b) Passive tension and stiffness of vertebrate skeletal and insect flight muscles: The contribution of weak cross-bridges and elastic filaments. *Biophys. J.* **65,** 2141-2159.

Greaser, M. (2001) Identification of new repeating motifs in titin. *Proteins* **43,** 145-149.

Gutierrez-Cruz, G., Van Heerden, A. and Wang, K. (2001) Modular motif, structural folds and affinity profiles of pevk segment of human fetal skeletal muscle titin. *J. Biol. Chem.* **276,** 7442-7449.

Hallett, P., Tskhovrebova, L., Trinick, J., Offer, G. and Miles, M. J. (1996) Improvements in atomic force microscopy protocols for imaging fibrous proteins. *J. Vac. Sci. Technol. B* **14,** 1444-1448.

Hansma, P. K., Elings, V. B., Marti, O. and Bracker, C. E. (1988) Scanning tunneling microscopy and atomic force microscopy: Application to biology and technology. *Science* **242,** 209-242.

Haravuori, H., Vihola, A., Straub, V., Auranen, M., Richard, I., Marchand, S., Voit, T., Labeit, S., Somer, H., Peltonen, L., Beckmann, J. S. and Udd, B. (2001) Secondary calpain3 deficiency in 2q-linked muscular dystrophy - titin is the candidate gene. *Neurology* **56,** 869-877.

Helm, C. A., Knoll, W. and Israelachvili, J. N. (1991) Measurement of ligand receptor interactions. *Proc. Natl. Acad. Sci. U. S. A.* **88,** 8169-8173.

Higuchi, H., Nakauchi, Y., Maruyama, K. and Fujime, S. (1993) Characterization of beta-connectin (titin 2) from striated muscle by dynamic light scattering. *Biophys. J.* **65,** 1906-1915.

Hinterdorfer, P., Baumgartner, W., Gruber, H. J., Schilcher, K. and Schindler, H. (1996) Detection and localization of individual antibody-antigen recognition events by atomic force microscopy. *Proc. Natl. Acad. Sci. U. S. A.* **93,** 3477-3481.

Horowits, R. (1999) The physiological role of titin in striated muscle. In *Rev. Physiol. Biochem. Pharm., Vol. 138*, pp. 57-96, Springer-Verlag Berlin, Berlin.

Horowits, R., Kempner, E. S., Bisher, M. E. and Podolsky, R. J. (1986) A physiological role for titin and nebulin in skeletal muscle. *Nature* **323,** 160-164.

Horowits, R., Maruyama, K. and Podolsky, R., J. (1989) Elastic behavior of connectin filaments during thick filament movement in activated skeletal muscle. *J. Cell Biol.* **109,** 2169-2176.

Hutter, J. L. and Bechhoefer, J. (1993) Calibration of atomic-force microscope tips. *Rev. Sci. Instrum.* **64,** 1868-1873.

Huxley, H. E. (1990) Sliding filaments and molecular motile systems. *J. Biol. Chem.* **265,** 8347-8350.

Izrailev, S., Stepaniants, S., Balsera, M., Oono, Y. and Schulten, K. (1997) Molecular dynamics study of unbinding of the avidin-biotin complex. *Biophys. J.* **72,** 1568-1581.

Jin, A. J., Forbes, J. G. and Wang, K. (2000) Atomic force microscopy studies of a titin pevk segment. *Biophys. J.* **78,** 381A.

Jin, A. J., Forbes, J. G. and Wang, K. (2001) Molecular elasticity of the pevk segment of titin: Entropic and enthalpic contributions. *Submitted*.

Keller, T. C. S. (1997) Muscle structure - molecular bungees. *Nature* **387,** 233-235.

Keller, T. C. S., Eilertsen, K., Higginbotham, M., Kazmierski, S., Kim, K. T. and Velichkova, M. (2000) Role of titin in nonmuscle and smooth muscle cells. In *Elastic filaments of the cell, Vol. 481*, pp. 265-281.

Kellermayer, M. S. Z., Smith, S., Bustamante, C. and Granzier, H. L. (2000) Mechanical manipulation of single titin molecules with laser tweezers. In *Elastic filaments of the cell, Vol. 481*, pp. 111-128.

Kellermayer, M. S. Z., Smith, S. B., Bustamante, C. and Granzier, H. L. (1998) Complete unfolding of the titin molecule under external force. *J. Struct. Biol.* **122,** 197-205.

Kellermayer, M. S. Z., Smith, S. B., Granzier, H. L. and Bustamante, C. (1997) Folding-unfolding transitions in single titin molecules characterized with laser tweezers. *Science* **276,** 1112-1116.

Klimov, D. K. and Thirumalai, D. (1999) Stretching single-domain proteins: Phase diagram and kinetics of force-induced unfolding. *Proc. Natl. Acad. Sci. U. S. A.* **96,** 6166-6170.

Klimov, D. K. and Thirumalai, D. (2000) Native topology determines force-induced unfolding pathways in globular proteins. *Proc. Natl. Acad. Sci. U. S. A.* **97,** 7254-7259.

Kramers, H. A. (1940) Brownian motion in a field of force and the diffusion model of chemical kinetics. *Physica* **7,** 284-304.

Krammer, A., Lu, H., Isralewitz, B., Schulten, K. and Vogel, V. (1999) Forced unfolding of the fibronectin type III module reveals a tensile molecular recognition switch. *Proc. Natl. Acad. Sci. U. S. A.* **96,** 1351-1356.

Kuo, S. C. (1998) A simple assay for local heating by optical tweezers. In *Methods in cell biology, Vol. 55*, (ed. M. P. Sheetz), pp. 43-45, Academic Press, San Diego.

Labeit, S. and Kolmerer, B. (1995) Titins - giant proteins in charge of muscle ultrastructure and elasticity. *Science* **270,** 293-296.

Leckband, D. (2000) Measuring the forces that control protein interactions. *Annu. Rev. Biophys. Biomolec. Struct.* **29,** 1-26.

Lee, G. U., Chrisey, L. A. and Colton, R. J. (1994) Direct measurement of the forces between complementary strands of dna. *Science* **266,** 771-773.

Levitt, M., Gerstein, M., Huang, E., Subbiah, S. and Tsai, J. (1997) Protein folding: The endgame. *Annu. Rev. Biochem.* **66,** 549-579.

Linke, W. A. (2000) Titin elasticity in the context of the sarcomere: Force and extensibility measurements on single myofibrils. In *Elastic filaments of the cell, Vol. 481*, pp. 179-206.

Linke, W. A., Ivemeyer, M., Mundel, P., Stockmeier, M. R. and Kolmerer, B. (1998) Nature of pevk-titin elasticity in skeletal muscle. *Proc. Natl. Acad. Sci. U. S. A.* **95,** 8052-8057.

Linke, W. A., Ivemeyer, M., Olivieri, N., Kolmerer, B., Ruegg, J. C. and Labeit, S. (1996) Towards a molecular understanding of the elasticity of titin. *J. Mol. Biol.* **261,** 62-71.

Linke, W. A., Rudy, D. E., Centner, T., Gautel, M., Witt, C., Labeit, S. and Gregorio, C. C. (1999) I-band titin in cardiac muscle is a three-element molecular spring and is critical for maintaining thin filament structure. *J. Cell Biol.* **146,** 631-644.

Liu, Y. Z., Leuba, S. H. and Lindsay, S. M. (1999) Relationship between stiffness and force in single molecule pulling experiments. *Langmuir* **15,** 8547-8548.

Lu, H., Isralewitz, B., Krammer, A., Vogel, V. and Schulten, K. (1998) Unfolding of titin immunoglobulin domains by steered molecular dynamics simulation. *Biophys. J.* **75,** 662-671.

Lu, H. and Schulten, K. (1999a) Steered molecular dynamics simulation of conformational changes of immunoglobulin domain I27 interpret atomic force microscopy observations. *Chem. Phys.* **247,** 141-153.

Lu, H. and Schulten, K. (1999b) Steered molecular dynamics simulations of force-induced protein domain unfolding. *Proteins: Struct., Funct., Genet.* **35,** 453-463.

Lu, H. and Schulten, K. (2000) The key event in force-induced unfolding of titin's immunoglobulin domains. *Biophys. J.* **79,** 51-65.

Ma, K., Kan, L. S. and Wang, K. (2001) Polyproline ii helix is a key structural motif of the elastic pevk segment of titin. *Biochemistry* **40,** 3427-3438.

Machado, C. and Andrew, D. J. (2000) Titin as a chromosomal protein. In *Elastic filaments of the cell, Vol. 481*, pp. 221-236.

Marko, J. F. and Siggia, E. D. (1995) Stretching DNA. *Macromolecules* **28,** 8759-8770.

Marszalek, P. E., Lu, H., Li, H. B., Carrion-Vazquez, M., Oberhauser, A. F., Schulten, K. and Fernandez, J. M. (1999) Mechanical unfolding intermediates in titin modules. *Nature* **402,** 100-103.

Maruyama, K. (1994) Connectin, an elastic protein of striated muscle. *Biophys. Chem.* **50,** 73-85.

Maruyama, K. (1997) Connectin/titin, giant elastic protein of muscle. *FASEB J.* **11,** 341-5.

Maruyama, K., Kimura, S., Ohashi, K. and Kuwano, Y. (1981) Connectin, an elastic protein of muscle. Identification of "titin" with connectin. *J. Biochem. (Tokyo)* **89,** 701-709.

Mehta, A. D., Rief, M., Spudich, J. A., Smith, D. A. and Simmons, R. M. (1999) Single-molecule biomechanics with optical methods. *Science* **283,** 1689-1695.

Merkel, R., Nassoy, P., Leung, A., Ritchie, K. and Evans, E. (1999) Energy landscapes of receptor-ligand bonds explored with dynamic force spectroscopy. *Nature* **397,** 50-53.

Minajeva, A., Kulke, M., Fernandez, J. M. and Linke, W. A. (2001) Unfolding of titin domains explains the viscoelastic behavior of skeletal myofibrils. *Biophys. J.* **80,** 1442-1451.

Moy, V. T., Florin, E. L. and Gaub, H. E. (1994) Intermolecular forces and energies between ligands and receptors. *Science* **266,** 257-259.

Muniz, J., Marin, J. L., Huerta, M., Del Rio, J., Larios, A. and Trujillo, X. (1999) Passive forces in mammalian skeletal muscle: A freely-jointed and worm-like chain. *Gen. Physiol. Biophys.* **18,** 155-163.

Nagao, E., Nishijima, H., Akita, S., Nakayama, Y. and Dvorak, J. A. (2000) The cell biological application of carbon nanotube probes for atomic force microscopy: Comparative studies of malaria- infected erythrocytes. *J. Electron Microsc.* **49,** 453-458.

Netzer, W. J. and Hartl, F. U. (1997) Recombination of protein domains facilitated by co-translational folding in eukaryotes. *Nature* **388,** 343-349.

Oberhauser, A. F., Marszalek, P. E., Carrion-Vazquez, M. and Fernandez, J. M. (1999) Single protein misfolding events captured by atomic force microscopy. *Nat. Struct. Biol.* **6,** 1025-1028.

Oberhauser, A. F., Marszalek, P. E., Erickson, H. P. and Fernandez, J. M. (1998) The molecular elasticity of the extracellular matrix protein tenascin. *Nature* **393,** 181-185.

Obermann, W. M., Plessmann, U., Weber, K. and Furst, D. O. (1995) Purification and biochemical characterization of myomesin, a myosin- binding and titin-binding protein, from bovine skeletal muscle. *Eur. J. Biochem.* **233,** 110-115.

Onuchic, J. N., LutheySchulten, Z. and Wolynes, P. G. (1997) Theory of protein folding: The energy landscape perspective. *Annu. Rev. Phys. Chem.* **48,** 545-600.

Ortiz, C. and Hadziioannou, G. (1999) Entropic elasticity of single polymer chains of poly(methacrylic acid) measured by atomic force microscopy. *Macromolecules* **32,** 780-787.

Paci, E. and Karplus, M. (1999) Forced unfolding of fibronectin type 3 modules: An analysis by biased molecular dynamics simulations. *J. Mol. Biol.* **288,** 441-459.

Paci, E. and Karplus, M. (2000) Unfolding proteins by external forces and temperature: The importance of topology and energetics. *Proc. Natl. Acad. Sci. U. S. A.* **97,** 6521-6526.

Pan, K.-M., Damodaran, S. and Greaser, M. L. (1994) Isolation and characterization of titin t1 from bovine cardiac muscle. *Biochemistry* **33,** 8255-8261.

Plaxco, K. W., Spitzfaden, C., Campbell, I. D. and Dobson, C. M. (1997) A comparison of the folding kinetics and thermodynamics of two homologous fibronectin type III modules. *J. Mol. Biol.* **270,** 763-770.

Rao, N. M., Plant, A. L., Silin, V., Wight, S. and Hui, S. W. (1997) Characterization of biomimetic surfaces formed from cell membranes. *Biophys. J.* **73,** 3066-3077.

Rief, M., Gautel, M., Oesterhelt, F., Fernandez, J. M. and Gaub, H. E. (1997a) Reversible unfolding of individual titin immunoglobulin domains by AFM. *Science* **276,** 1109-1112.

Rief, M., Gautel, M., Schemmel, A. and Gaub, H. E. (1998) The mechanical stability of immunoglobulin and fibronectin III domains in the muscle protein titin measured by atomic force microscopy. *Biophys. J.* **75,** 3008-3014.

Rief, M., Oesterhelt, F., Heymann, B. and Gaub, H. E. (1997b) Single molecule force spectroscopy on polysaccharides by atomic force microscopy. *Science* **275,** 1295-1297.

Rohs, R., Etchebest, C. and Lavery, R. (1999) Unraveling proteins: A molecular mechanics study. *Biophys. J.* **76,** 2760-2768.

Sader, J. E., Chon, J. W. M. and Mulvaney, P. (1999) Calibration of rectangular atomic force microscope cantilevers. *Rev. Sci. Instrum.* **70,** 3967-3969.

Sader, J. E., Larson, I., Mulvaney, P. and White, L. R. (1995) Method for the calibration of atomic-force microscope cantilevers. *Rev. Sci. Instrum.* **66,** 3789-3798.

Shao, Z. F., Mou, J., Czajkowsky, D. M., Yang, J. and Yuan, J. Y. (1996) Biological atomic force microscopy: What is achieved and what is needed. *Adv. Phys.* **45,** 1-86.

Shao, Z. F., Yang, J. and Somlyo, A. P. (1995) Biological atomic force microscopy: From microns to nanometers and beyond. *Annu. Rev. Cell Dev. Biol.* **11,** 241-265.

Shtilerman, M., Lorimer, G. H. and Englander, S. W. (1999) Chaperonin function: Folding by forced unfolding. *Science* **284,** 822-825.

Smith, S. B., Cui, Y. J. and Bustamante, C. (1996) Overstretching b-DNA: The elastic response of individual double-stranded and single-stranded DNA molecules. *Science* **271,** 795-799.

Socci, N. D., Onuchic, J. N. and Wolynes, P. G. (1999) Stretching lattice models of protein folding. *Proc. Natl. Acad. Sci. U. S. A.* **96,** 2031-2035.

Sorimachi, H., Ono, Y. and Suzuki, K. (2000) Skeletal muscle-specific calpain, p94, and connectin/titin: Their physiological functions and relationship to limb-girdle muscular dystrophy type 2a. In *Elastic filaments of the cell, Vol. 481*, pp. 383-397.

Soteriou, A., Gamage, M. and Trinick, J. (1993) A survey of interactions made by the giant protein titin. *J. Cell Sci.* **104,** 119-123.

Strick, T. R., Allemand, J. F., Bensimon, D. and Croquette, V. (2000) Stress-induced structural transitions in DNA and proteins. *Annu. Rev. Biophys. Biomolec. Struct.* **29,** 523-543.

Strunz, T., Oroszlan, K., Schumakovitch, I., Guntherodt, H. J. and Hegner, M. (2000) Model energy landscapes and the force-induced dissociation of ligand-receptor bonds. *Biophys. J.* **79,** 1206-1212.

Svoboda, K. and Block, S. M. (1994) Biological applications of optical forces. In *Annu. Rev. Biophys. Biomolec. Struct., Vol. 23*, (eds. R. M. Stroud, C. R. Cantor and T. D. Pollard), pp. 247-285, Annual Reviews, Inc., Palo Alto, CA.

Trinick, J. and Tskhovrebova, L. (1999) Titin: A molecular control freak. *Trends Cell Biol.* **9,** 377-380.

Trombitas, K., Greaser, M., Labeit, S., Jin, J. P., Kellermayer, M., Helmes, M. and Granzier, H. (1998) Titin extensibility in situ: Entropic elasticity of permanently folded and permanently unfolded molecular segments. *J. Cell Biol.* **140,** 853-859.

Trombitas, K. and Pollack, G. H. (1993) Elastic properties of connecting filaments along the sarcomere. *Adv. Exp. Med. Biol.* **332,** 71-79.

Tskhovrebova, L., Trinick, J., Sleep, J. and Simmons, R. (1996) Optical tweezer measurements of force and extension in individual titin molecules. *J. Muscle Res. Cell Motil.* **17,** 113-113.

Tskhovrebova, L., Trinick, J., Sleep, J. A. and Simmons, R. M. (1997) Elasticity and unfolding of single molecules of the giant muscle protein titin. *Nature* **387,** 308-312.

Tsuda, Y., Yasutake, H., Ishijima, A. and Yanagida, T. (1996) Torsional rigidity of single actin filaments and actin-actin bond breaking force under torsion measured directly by in vitro micromanipulation. *Proc. Natl. Acad. Sci. U. S. A.* **93,** 12937-12942.

van der Ven, P. F. M., Wiesner, S., Salmikangas, P., Auerbach, D., Himmel, M., Kempa, S., Hayess, K., Pacholsky, D., Taivainen, A., Schroder, R., Carpen, O. and Furst, D. O. (2000) Indications for a novel muscular dystrophy pathway: Gamma- filamin, the muscle-specific filamin isoform, interacts with myotilin. *J. Cell Biol.* **151,** 235-247.

Viani, M. B., Schaffer, T. E., Chand, A., Rief, M., Gaub, H. E. and Hansma, P. K. (1999a) Small cantilevers for force spectroscopy of single molecules. *J. Appl. Phys.* **86,** 2258-2262.

Viani, M. B., Schaffer, T. E., Paloczi, G. T., Pietrasanta, L. I., Smith, B. L., Thompson, J. B., Richter, M., Rief, M., Gaub, H. E., Plaxco, K. W., Cleland, A. N., Hansma, H. G. and Hansma, P. K. (1999b) Fast imaging and fast force spectroscopy of single biopolymers with a new atomic force microscope designed for small cantilevers. *Rev. Sci. Instrum.* **70,** 4300-4303.

Visscher, K. and Block, S. M. (1998) Versatile optical traps with feedback control. In *Molecular motors and the cytoskeleton, pt b, Vol. 298*, pp. 460-489.

Visscher, K., Gross, S. P. and Block, S. M. (1996) Construction of multiple-beam optical traps with nanometer- resolution position sensing. *Ieee Journal of Selected Topics in Quantum Electronics* **2,** 1066-1076

Wang, K. (1982) Purification of titin and nebulin. *Methods Enzymol.* **85,** 264-274.

Wang, K. (1996) Titin/connectin and nebulin: Giant protein rulers of muscle structure and function. *Adv. Biophys.* **33,** 123-34.

Wang, K. (1999) Titin. In *Guidebook to the cytoskeletal and motor proteins*, (eds. T. Kries and R. Vale), pp. 481-486, Oxford University Press, Oxford.

Wang, K., McCarter, R., Wright, J., Beverly, J. and Ramirez-Mitchell, R. (1991) Regulation of skeletal muscle stiffness and elasticity by titin isoforms: A test of the segmental extension model of resting tension. *Proc. Natl. Acad. Sci. U. S. A.* **88,** 7101-7105.

Wang, K., McCarter, R., Wright, J., Beverly, J. and Ramirez-Mitchell, R. (1993) Viscoelasticity of the sarcomere matrix of skeletal muscles: The titin-myosin composite filament is a dual-stage molecular spring. *Biophys. J.* **64,** 1161-1177.

Wang, K., McClure, J. and Tu, A. (1979) Titin: Major myofibrillar components of striated muscle. *Proc. Natl. Acad. Sci. USA* **76,** 3698-3702.

Wang, K., Ramirez-Mitchell, R. and Palter, D. (1984) Titin is an extraordinarily long, flexible, and slender myofibrillar protein. *Proc. Natl. Acad. Sci. U. S. A.* **81,** 3685-3689.

Wang, K., Wright, J., Gutierrez, G., Brady, A. and Sheetz, M. (1997a) Titin elasticity: Laser trap measurement of force-extension curves of isolated titin molecules. *Biophys. J.* **72,** MAMA6.

Wang, M. D., Schnitzer, M. J., Yin, H., Landick, R., Gelles, J. and Block, S. M. (1998) Force and velocity measured for single molecules of rna polymerase. *Science* **282,** 902-907.

Wang, M. D., Yin, H., Landick, R., Gelles, J. and Block, S. M. (1997b) Stretching DNA with optical tweezers. *Biophys. J.* **72,** 1335-1346.

Weiss, S. (1999) Fluorescence spectroscopy of single biomolecules. *Science* **283,** 1676-1683.

Whiting, A., Wardale, J. and Trinick, J. (1989) Does titin regulate the length of muscle thick filaments? *J. Mol. Biol.* **205,** 263-268.

Woolley, A. T., Guillemette, C., Cheung, C. L., Housman, D. E. and Lieber, C. M. (2000) Direct haplotyping of kilobase-size DNA using carbon nanotube probes. *Nat. Biotechnol.* **18,** 760-763.

Yang, G. L., Cecconi, C., Baase, W. A., Vetter, I. R., Breyer, W. A., Haack, J. A., Matthews, B. W., Dahlquist, F. W. and Bustamante, C. (2000) Solid-state synthesis and mechanical unfolding of polymers of T4 lysozyme. *Proc. Natl. Acad. Sci. U. S. A.* **97,** 139-144.

Yasuda, R., Miyata, H. and Kinosita, K. (1996) Direct measurement of the torsional rigidity of single actin filaments. *J. Mol. Biol.* **263,** 227-236.

Zhang, B., Xu, G. Z. and Evans, J. S. (1999) A kinetic molecular model of the reversible unfolding and refolding of titin under force extension. *Biophys. J.* **77,** 1306-1315.

Zheng, X. Y., Ding, Y. Z., Bottomley, L. A., Allison, D. P. and Warmack, R. J. (1995) Discontinuous gold island films on mica. *J. Vac. Sci. Technol. B* **13,** 1320-1324.

Zhuang, X. W., Ha, T., Kim, H. D., Centner, T., Labeit, S. and Chu, S. (2000) Fluorescence quenching: A tool for single-molecule protein- folding study. *Proc. Natl. Acad. Sci. U. S. A.* **97,** 14241-14244.

Zlatanova, J., Lindsay, S. M. and Leuba, S. H. (2000) Single molecule force spectroscopy in biology using the atomic force microscope. *Prog. Biophys. Mol. Biol.* **74,** 37-61.

Figure captions:

Fig. 1: Elasticity and segmental extension of sarcomere associated cytoskeletons.
(A) Proposed structural changes in titin/myosin composite filaments upon stretching. (B) Resting tension-sarcomere length relationship of myofibrillar bundles containing both sarcomere matrix and intermediate filaments. Straightening of slack titin filaments at low tension (Zone I) is followed by the extension of the I band segment of titin/myosin composite filaments that gives rise to the exponential rise in tension (ERT) (zone II, between SL_e and SL_y). The detachment of part of the anchored titin segment at and beyond the elastic limit (yield point) of the sarcomere (Sl_y) contributes to the leveling of tension at higher degrees of stretch (zone III). Stretching of intermediate filament lattice contributes to the further increase in tension beyond 5 μm (zone IV). The resting tension curves of several types of muscles with different titin isoforms and elastic limits can be normalized to the same master curve by plotting resting tension as a function of the degree of stretch of the extensible segment of titin (extensible segmental ratio in B). (C) The mechanical unfolding or "yielding" of Ig and/or Fn3 domains that adjusts length and spring constant of the titin molecule. (D). The extension of the intermediate filaments that surround the sarcomeres and insert at the force-bearing structures at the Z line and M lines. The intermediate filaments provide mechanical continuity of the myofibril even when individual sarcomere is damaged. The segmental elasticity of titin and sarcomere is correlated closely to the extension of its rich molecular motifs such as the PEVK segment (marked in A as unfolded strings) and the Ig/Fn3 domains (marked in A as folded beads), see Fig. 2 and the text. (See Wang *et al.* (1993) for more details and the figure was adopted with permission from *Biophysical Journal*.)

Fig. 2: Schematic diagrams of titin motifs and myofibril elasticity.
(A) Differential motifs and splicing pathways of titin in the extensible I-band. Adopted from Freiburg *et al.* (2000) with permission from American Heart Association and Lippincott Williams & Wilkins. Identified splice routes are indicated by arrows, black for human and blue for rabbit. Predicted molecular weights of respective isoforms are given (right). All isoforms share the I27 exon and I84 exon (see bottom row). These alternative splicings for skeletal titins and cardiac N2-A titin are in combinations of additional 53 Ig domains (red), N2-B to N2-A (red-blue) substitution, and variable PEVK sequence length (yellow). All skeletal titins have the 53 Ig

domain additions and variable PEVK length (with, e.g. 2174 residues in human soleus). Cardiac N2-A titin has a shorter extendable N2 insertion sequence, but a larger PEVK length. The details of Z-line, A-band and M-line motifs are not shown (see, e.g., (Freiburg *et al.*, 2000; Labeit and Kolmerer, 1995)). (B) Segmental extension of titin motifs (after Wang *et al.* (1991)). Passive-force and sarcomere extension curves from most muscle types all scale to a multi-stage master relationship. The defining characteristics of the force curves are mainly the total lengths of the extensible Ig-motifs, which set the length SL_E-SL_O, and the unique sequences (PEVK plus N2-B and/or N2-A), which set the length SL_Y-SL_E and the strength of titin/myosin interaction which determines the yield point (SL_Y). The multistage passive tension *vs.* sarcomere I-band extension are attributed to the straightening of Ig-motifs (low force), the unique insertions such as PEVK and N2-A/B (exponential rising force), and the participation of newly recruited Fn3 motifs from the thick filament segment (beyond the yield point force, F_Y). See text for further details.

Fig. 3: Molecular morphology of native titin (T2) by rotary shadowing electron microscopy.
(A) Highly convoluted titin strands (0.5 M ammonium formate buffer) (bar = 1 μm). Note the flexible beaded string that twists and turns sharply (Inset. bar = 0.2 μm). (B) Linearized titin strands on tilt-sprayed mica (0.5 M KCl buffer). Hydrodynamic shear force linearized the flexible titin strands. Note the multi-stranded regions (ms) and the nodules (n). (bar = 1 μm). (C) High-magnification view selected from (B). Note the relative dimension of titin and myosin (my). The beaded string morphology is less conspicuous in this image and the titin strands appear uniform in width (bar =0.2 μm). (D) Reticular network and stretching of titin strands (in 0.5 M KCl). Note the thinning of many strands (brackets) (bar = 1 μm). (E) Selected high-magnification view of (D). Note the different thickness of these strands and the irregularly spaced beads (arrowheads), reflecting the unfolding of titin domains (bar = 0.2 μm). Figure after Fig. 2 in Wang *et al.* (1984) with permission, and more details may be found therein.

Fig. 4. Effects of applied force in weak interactions.
(A) Idealized interaction potential with transition states. A force applied at an angle θ to the reaction coordinate x, adds a mechanical potential $-(f\cos\theta)x$, which tilts the reaction landscape and lowers the barrier. The energy contours near the transition states are highly curved and their shape and position are not affected significantly by the applied force. The transition states at low and high forces are indicated by x_u.

(B) Force histograms from measurements on single biotin-streptavidin interactions at different loading rates. Solid curves are Gaussian fits used to determine the center of the force peak. This plot demonstrates the shift in the peak position and the increasing peak width with increasing loading rate.

(C) Dynamic strength spectra for biotin-avidin and biotin-streptavidin interactions. Three distinct regions are seen for biotin-avidin, whereas only two are seen for biotin-streptavidin. At lower loading rates, the interactions are dominated by the outer barriers. See Merkel *et al.* (1999) for more details. Panels (A-C) were modified from Merkel *et al.* (1999) with permission from *Nature*.

(D) Histogram of unfolding forces for an octamer of I27 Ig domains in a polymer stretched with an AFM, adapted from Carrion-Vazquez *et al.* (1999b) with permission from *Proc. Natl. Acad. Sci. U. S. A.* The solid curves are Monte-Carlo simulations of the mean unfolding force of the I27 polymer with different unfolding lifetimes, an unfolding distance of 0.25 nm and a pulling rate of 0.6 nm/ms. This plot demonstrates that the bond-strength (the peak in the histogram) is sensitive to both the loading rate and the bond lifetime.

Fig. 5: Elasticity models for titin and sarcomere extension.

(A) Worm-like chain model (WLC, left) and freely-jointed chain (FJC, right) model for the force-extension curves of titin molecules.

(B) Normalized tension plots based on three models of titin extension (ERT, WLC and FLC). Note that these models are indistinguishable and equally applicable to explain the tension-length curve of the sarcomere below a fractional extension of about 0.8. Model equations and parameters (see Table 1) for normalizing force at the fractional extensions of 0.35 and 0.7 are as follows (Jin, Forbes, and Wang, unpublished result):

a): ERT $(E_0/\alpha \cong 0.260, \alpha/TLE_0 = 1.856)$

b): WLC $(k_BT/p = 1,1/L_0 = 1,1/K_0 = 0)$

c): WLC $(k_BT/p = 0.972,1/L_0 = 1.030,1/K_0 = 0.005)$

d): FJC $(k_BT/L_K \cong 0.957,1/L_0 \cong 1.217,1/K_0 = 0)$

e): FJC $(k_BT/L_K \cong 0.918,1/L_0 \cong 1.265,1/K_0 = 0.01)$

Fig. 6: Instrument design

(A) Atomic Force Microscope. (B) Laser Optical Trap from Bennink *et al.* (1999) with permission from *Wiley-Liss Inc.*, a subsidiary of *John Wiley & Sons, Inc*. See text for the details.

Fig. 7: Attachment methods for the extension of native titin.

(A) AFM. Native titin is adsorbed onto gold surface and then picked up by pressing the tip onto the surface. A portion of titin becomes adsorbed onto the tip. This attachment gives rise to an extension curve as the tip is lifted from the surface.

(B) LOT: Attachment method used by Kellermayer and colleagues for stretching native titin. The Z-line end is attached to a 3 μm bead *via* the T12 antibody. The M-line end is attached to a silica bead coated with myomesin. Figure from Kellermayer *et al.* (1998) with permission from *Academic Press*.

(C) LOT: Attachment method used by Tskhovrebova and colleagues (Tskhovrebova *et al.*, 1997). The Z-line end was attached *via* the T12 antibody and the M-line end *via* the AB5 antibody. Figure from Tskhovrebova *et al.* (1997) with permission from *Nature*.

Fig. 8: Representative data from the different methods of investigating titin elasticity.

(A) Force-extension of native rabbit skeletal muscle titin by an optical trap (Tskhovrebova *et al.*, 1997), with permission from *Nature*. The experiment data (solid line) are fitted with either a single component WLC model (dotted line) or a two-component WLC model (open circles).

(B) Stepwise stress-relaxation of native rabbit skeletal muscle titin by an optical trap (Tskhovrebova *et al.*, 1997). The titin was stretched in 250 nm steps and then allowed to relax for over 1 s. When the force reached 120 pN, domains began to unfold to give rise to the staircase pattern (Tskhovrebova *et al.*, 1997), with permission from *Nature*.

(C) Extension of native rabbit skeletal muscle titin by an optical trap (figure from Kellermayer *et al.* (1998) with permission of *Academic Press*). In the trap, titin molecule straightens and PEVK extends in A and titin Ig/Fn3 domains start to unfold between A and B. Complete unfolding of titin domains from B to C gives rise to a curve that is well-fit with the WLC model of chain dynamics. Upon release, the completely unfolded titin polypeptide chain behaves as a worm like chain.

(D) Extension of native human cardiac titin (figure with permission from Rief *et al.* (1997a), copyright [1997] *American Association for Advancement of Science*). The striking sawtooth

patterns at high force reflect the sequential unfolding of titin Ig/Fn3 domains under stress. Notice the long extensions in the lower two extension curves, which indicate the extension of a portion of the protein before domains unfold.

(E) Cartoon of the relationship between the structure of the extended titin domains and positions on the force curve (figure with permission from Erickson (1997), copyright [1997] American Association for Advancement of Science). Lettering on the force curve in the inset corresponds with possible structures of the titin filament at these extensions.

Table 1: Equations for titin elasticity and their behaviors at low (a), medium (b), and high (c) force stretching.

Exponential Resting Tension (ERT)	$f = E_0 \alpha^{-1} \cdot \left(e^{\alpha \cdot \varepsilon} - 1\right)$ $(a) f \approx E_0 \cdot \varepsilon \qquad (b) f \approx \frac{E_0}{\alpha} \cdot \left(e^{\alpha/2} - 1\right) \qquad (c) f \approx E_0 \cdot \alpha^{-1} \cdot e^{\alpha \cdot \varepsilon}$
Enhanced Worm-like Chain (WLC)	$f = \frac{k_B T}{p}\left(\frac{1}{4 \cdot \left(1 - \ell / L_0 + f / K_0\right)^2} - \frac{1}{4} + \ell / L_0 - f / K_0\right)$ $(a) f \approx 3 \cdot \frac{k_B T}{2 \cdot p} \cdot \frac{\ell}{L_0} \qquad (b) f \approx 2.5 \cdot \frac{k_B T}{2 \cdot p} \qquad (c) f \approx K_0 \cdot (\ell / L_0 - 1)$
Enhanced Freely-Jointed Chain (FJC)	$\ell / L_0 = \left(\coth(\frac{L_K \cdot f}{k_B \cdot T}) - \frac{k_B \cdot T}{L_K \cdot f}\right) \cdot (1 + f / K_0)$ $(a) f \approx 3 \cdot \frac{k_B T}{L_K} \cdot \frac{\ell}{L_0} \qquad (b) f \approx 1.8 \cdot \frac{k_B T}{L_K} \qquad (c) f \approx K_0 \cdot (\ell / L_0 - 1)$

(a) Low force, ε, $\ell / L_0 << 1$.

(b) Medium force ε, $\ell / L_0 \approx 1/2$.

(c) High ε, $\ell / L_0 > 1$.

See also Fig. 5 and the text.

Table 2: Comparison of atomic force microscopy (AFM) and laser optical trap (LOT).

	Atomic Force Microscopy	**Laser Optical Trap**
Force Generation	Bending of cantilever obeys Hooke's Law	Intensity gradient from photons from laser light source
Dynamic range	20pN – >20nN with different cantilevers	0.1 – 400 pN[a]
Speed of extension	10 nm/s – 100 μm/s	10 nm/s – 100 μm/s
Force Constant	Typically 0.05 N/m	Typically 0.0002N/m
Loading Rate	0.5 - 5000 nN/s	0.002 – 2.0 nN/s
Calibration	• Thermal Fluctuation[b] • Added mass[d] • Cantilever dimensions and oscillation [f]	• Hydrodynamic drag[c] • Power Spectrum and equipartition theorem[e] • Secondary reference, i.e. extension of DNA[g]
Strengths	• Atomic resolution images • Large dynamic force range and small contact area • Compact instrument • Reliable calibration • Fast application of force	• Gentle, small forces • Increase force by turning up laser power • Simultaneous observation of sample motion and force response • Multiple traps available
Limitations	• Cantilever must be switched to change force range	• Large contact area of bead • Potential heating of sample
Instrumentation	• Many companies offering imaging and force measuring microscopes • Z-axis force measuring instruments	• Mainly custom built systems using research grade optical microscope, IR laser, and laser optics

[a]Kellermayer et al. (1998, 1997) and Tskhovrebova et al. (1997).
[b]Hutter and Bechhoefer (1993).
[c]Bennink et al. (1999).
[d]Cleveland et al. (1993).
[e]Svoboda and Block (1994).
[f]Sader et al. (1999, 1995).
[g]Wang et al. (1997b).

Table 3. Main observations of single molecule measurements of titin and titin motifs using AFM and LOT.

	Atomic Force Microscopy	**Laser Optical Trap**
Titin	Bovine cardiac [a]	Rabbit *longissimus dorsi*[b,c]
Recombinant proteins	• Human cardiac Ig domains [a, d, e, f, g] • Human skeletal Ig and Fn3 domains[h]	N/A
Assay Buffer	• Phosphate Buffered Saline (pH 7.4) • 10 mM imidazole, 10 mM K-EGTA, 2.5 mM $MgCl_2$, 2 mM NaN_3, pH 7.0, variable $CaCl_2$ for pCa = 3- 8, variable KCl for ionic strength = 35-560 mM[n]	• 25 mM imidazole, 25 mM KCl, 4 mM $MgCl_2$, 1 mM EGTA, 1 mM DTT, pH 7.4, 0.2% TWEEN, 0.2 mg/ml T4 lysozyme, 42 μM leupeptin, 10 μM E-64[b] • 19 mM histidine, 0.3 M KCl, 0.1 mM NaN3, 1 mM EGTA 0.1 mM DTT, pH 7.5[c]
Protein attachment	• Native titin 10-100 μg/ml in PBS. Deposited onto freshly evaporated gold surface, incubated for 10 min [a] • Recombinant fragments are cysteine labeled for covalent attachment to gold surface. Deposited from a 10-100 μg/ml solution in PBS. Protein film was 20-50 nm thick[e] • Tip was pressed into the surface and the protein adsorbed onto the tip at random positions.	• Native titin Z-line end attached to a 3 μm polystyrene sphere via the T12 antibody[i,j]. Specific attachment. • M-line end attached to a glass bead via myomesin on a 2μm glass bead[b,j, k]. Frequently bound nonspecifically to various positions on molecule. • Attached to a glass surface via the AB5 antibody[c,l]

- **Observations**

Extension of native titin

- Variable length spacer region followed by a sawtooth pattern.
- Peaks were spaced 25-38 nm apart with forces between 150-300pN.
- Sawtooth pattern resulted from unfolding of IG and Fn3 domains.
- Refolding observed in repeated extension-retraction cycles.
- Force required for unfolding was speed dependent.[a]

Extension of recombinant titin segments

- Sawtooth patterns observed with the number of teeth up to the number of domains in fragment.
- Different domain types had different mechanical stabilities and unfolded at different forces [h].
- Unfolding folding rate at zero force was 3.3×10^{-4} s^{-1}.
- Length of polymer contracted by 23 Å upon folding.
- Unfolding energy barrier height for mechanical and chemical unfolding were similar.
- Refolding was slower for mechanically unfolded proteins due to entropy loss and increased folding barrier[m]
- Mutations in load bearing portion of protein were identified by forced unfolding[e]
- Ig domains underwent a 6.6 Å transitional extension at 100 pN, resulting from the rupture of hydrogen bonds between the A and B β-strands of the Ig domain.
- Extension disappeared in a mutant where the H-bonds cannot form[f]
- Repeated unfolding and folding resulted in the aggregation of two misfolding domains and 'skips' in the unfolding pattern [g]

- Dynamic force-extension [c]
- Monotonic extension curves reflect worm-like chains.
- Static force-extension[b,c,j]
- Stretch-release hysteresis loops increased in width with degree of stretch and repeated stretching at constant length.
- Titin refolding force plateaued at low-force of 2-3 pN[b]
- Step-wise relaxation of stress when length change was held constant indicated domain unfolding.[c]

[a]Rief *et al.* (1997a).

[b]Kellermayer *et al.* (1997).
[c]Tskhovrebova *et al.* (1997).
[d]Carrion-Vazquez *et al.* (1999b).
[e]Carrion-Vazquez *et al.* (1999a).
[f]Marszalek *et al.* (1999).
[g]Oberhauser *et al.* (1999).
[h]Rief *et al.* (1998).
[i]Furst *et al.* (1988).
[j]Kellermayer *et al.* (1998).
[k] Obermann *et al.* (1995).
[l] Whiting *et al.* (1989).
[m] Carrion-Vazquez *et al.* (1999b).
[n] Jin *et al.* (2001).

Table 4: Summary of the persistence lengths for titin and titin motifs.

Proteins	Persistence Length (WLC, nm)	Experimental conditions
Titin	0.15 ±0.1[a] (PEVK/N2)	• LOT. Two segment fits. Force range 0 to 60 pN. Room Temperature. In 0.3 M KCl.
	4.6 ± 0.9[a] (Ig/Fn3)	• FJC fits gave a corresponding Kuhn length values of 0.35 ± 0.03 nm (PEVK) and 5.3 ± 0.08 nm (Ig/Fn3 domains).
	1.5-2.0[b,c]	• LOT. Attributed to the "fully unfolded T1." Single-segment WLC fits only and contour length was only 4 μm. 1-3 titin stretched each time and the *Lp* value distributed accordingly. About 60 mM buffer ionic strength, low Ca^{2+}.
	15[f]	• Dynamic light scattering. T2 with folded Ig/Fn3 in 0.3 M NaCl and 0.25 M potassium Phosphate buffer (pH =7.0).
Poly-Ig recombinant	0.4[d]	• AFM. Leading edges of titin Ig8 sawtooth-like stretch curves. In 200 mM PBS over Au surface at room temperature, low Ca^{2+}.
PEVK recombinant	0.3-0.7[e]	• AFM. 51 kDa PEVK cloned segment. Ca^{2+} and ionic strength dependency.

[a]Tskhovrebova *et al.* (1997).

[b]Kellermayer *et al.* (1998).

[c]Kellermayer *et al.* (1997)

[d]Rief *et al.* (1997a).

[e]Jin *et al.* (2001).

[f]Higuchi *et al.* (1993)

Fig.1: Wang, et al.

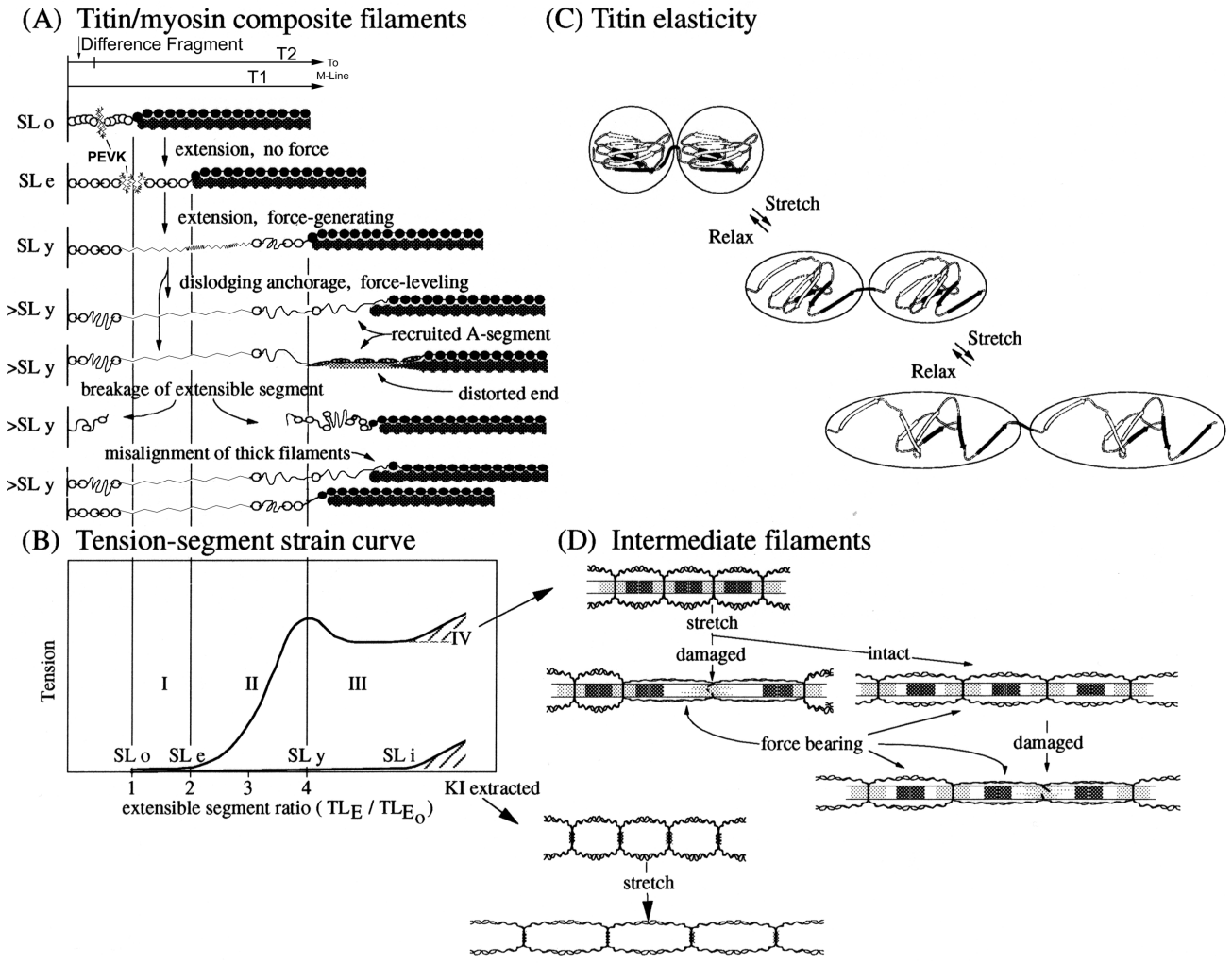

Fig. 2: Wang, et al. {Reproduction in color}

(A)

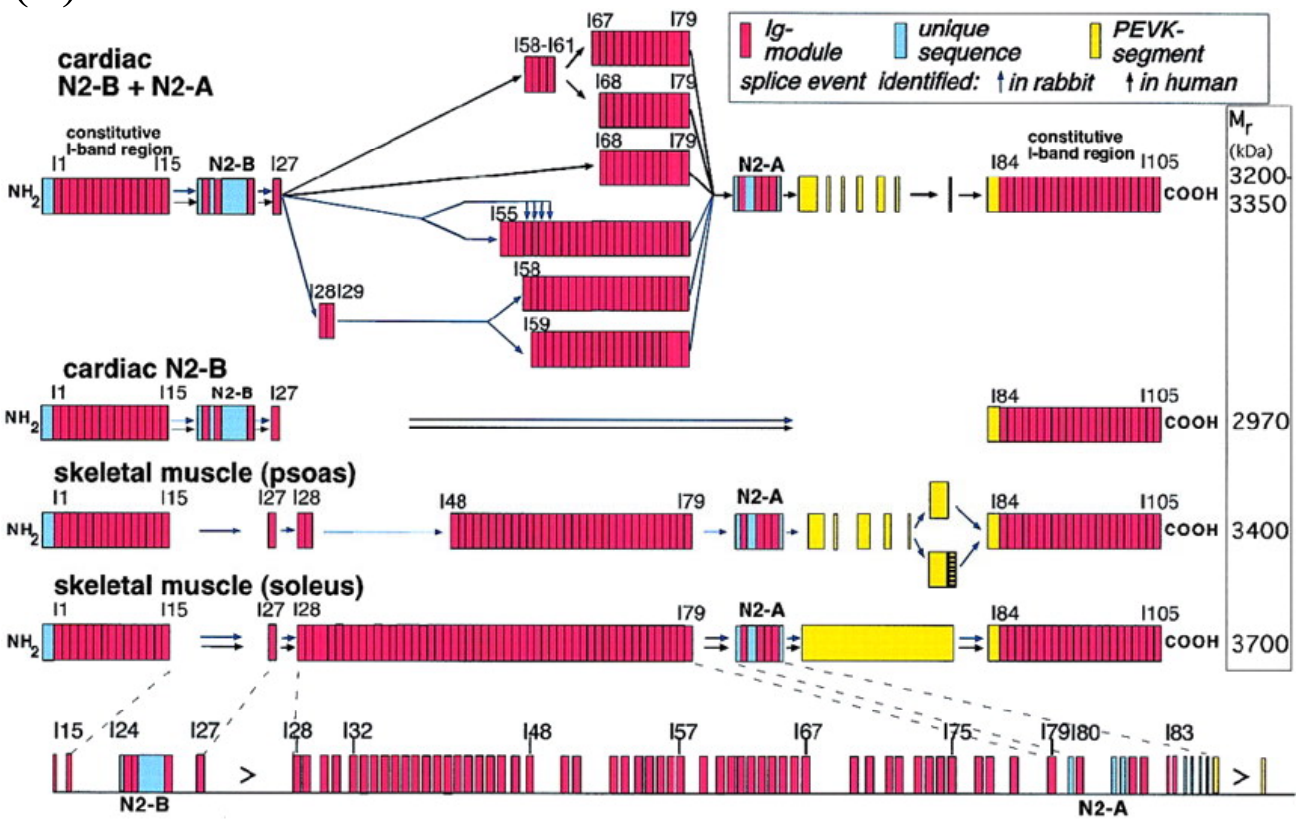

(B)

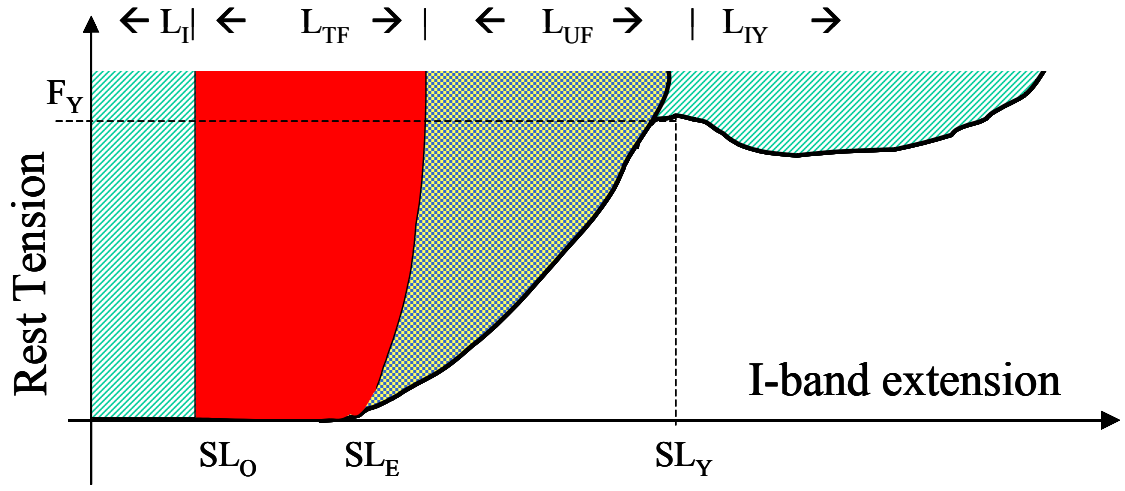

Fig. 3. Wang, et al.

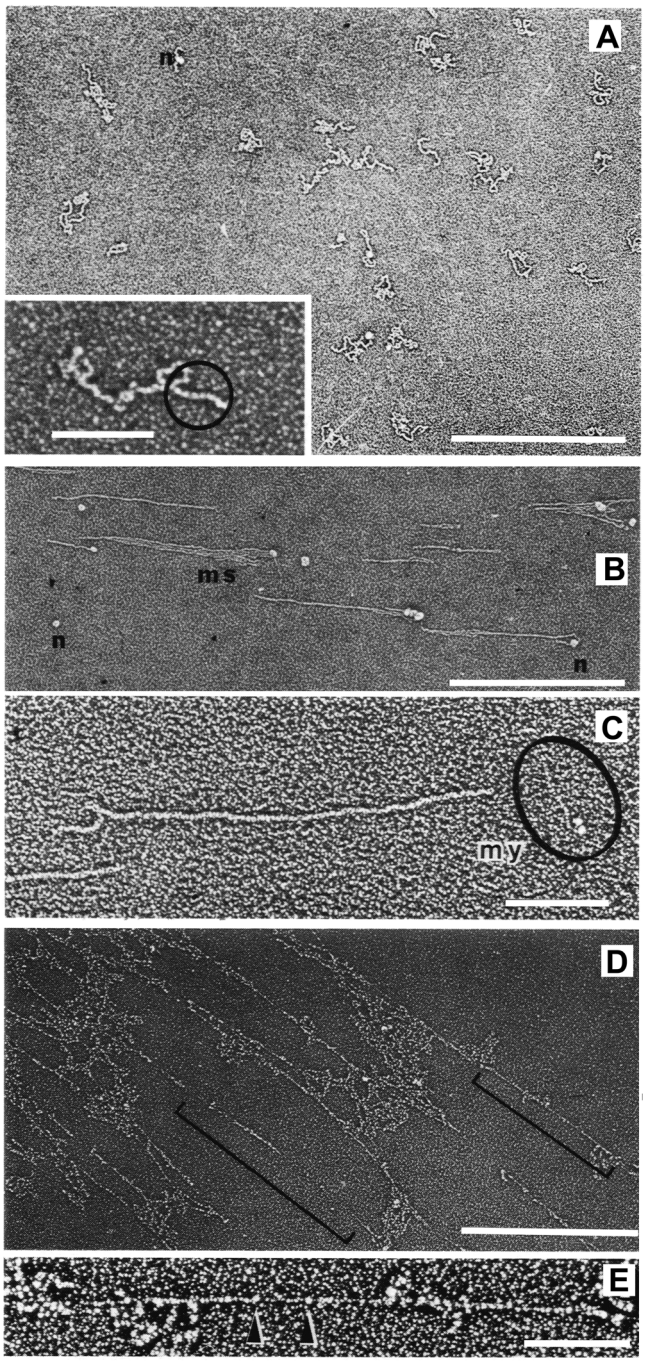

Fig.4: Wang, et al.

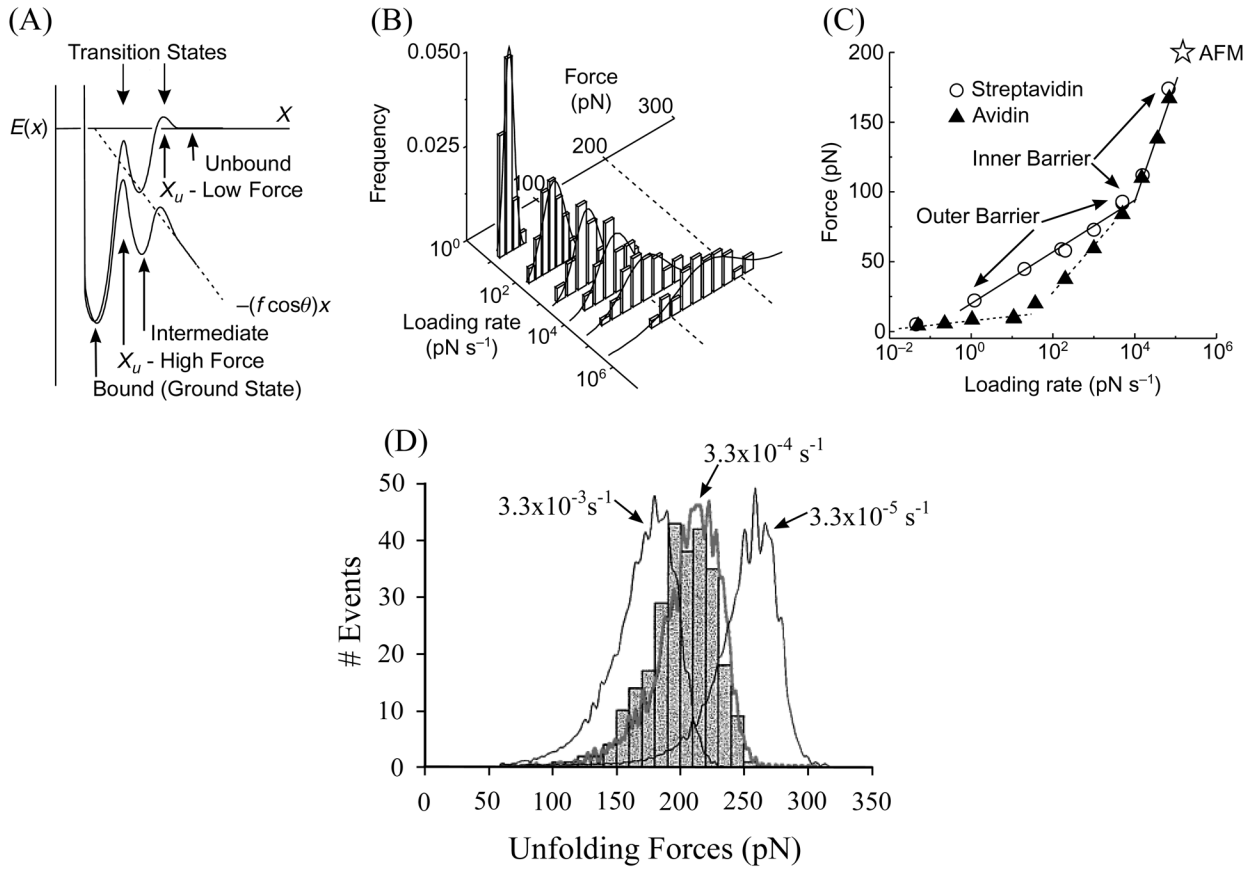

Fig.5: Wang, et al.

(A)

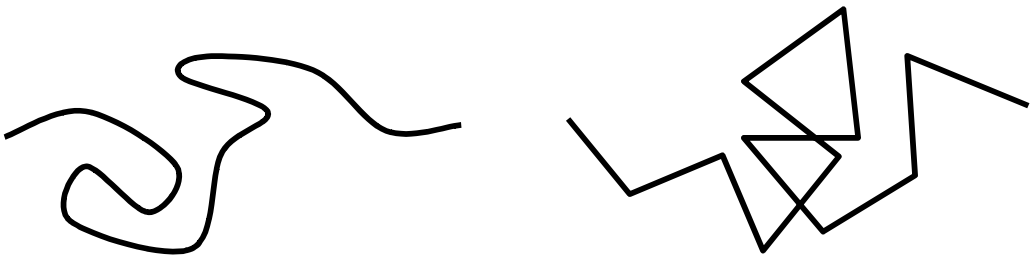

(B)

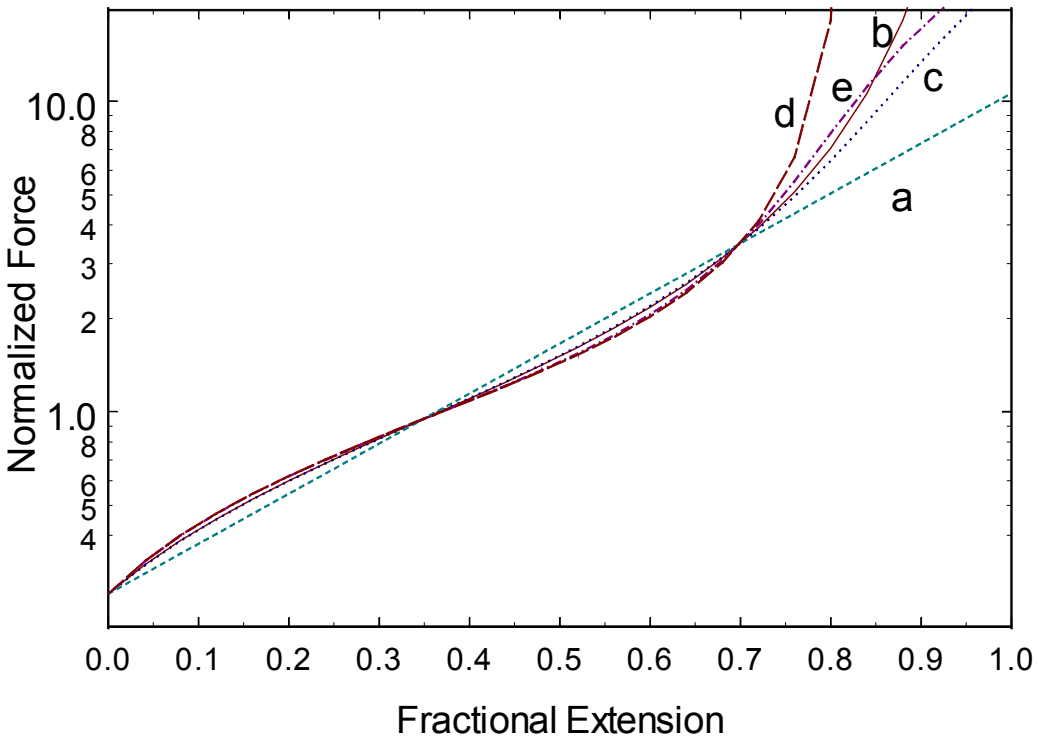

Fig.6: Wang, et al.

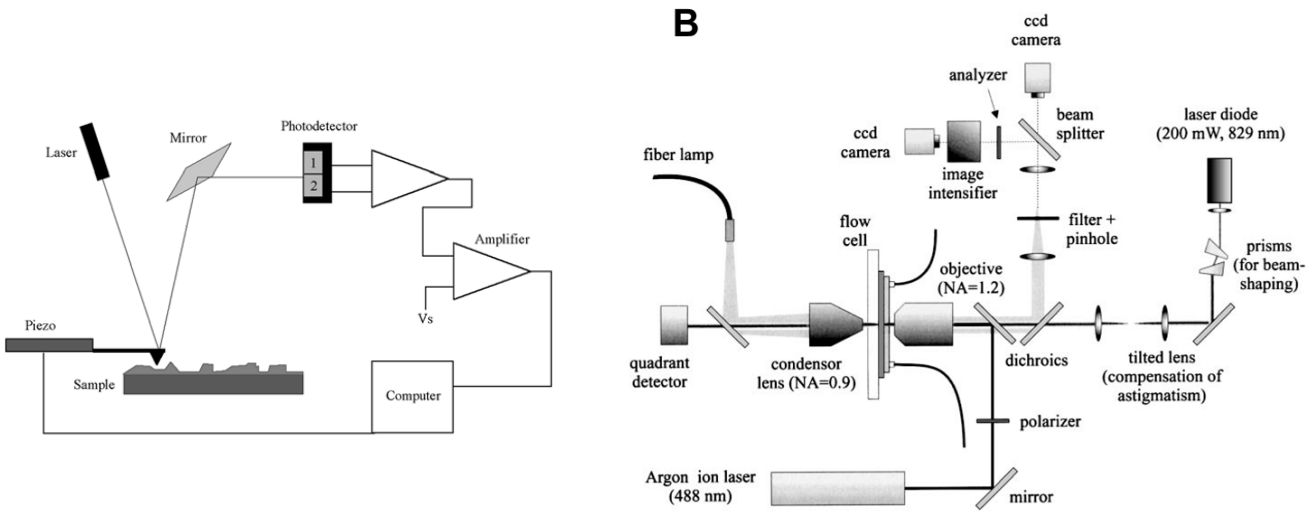

Fig.7: Wang, et al.

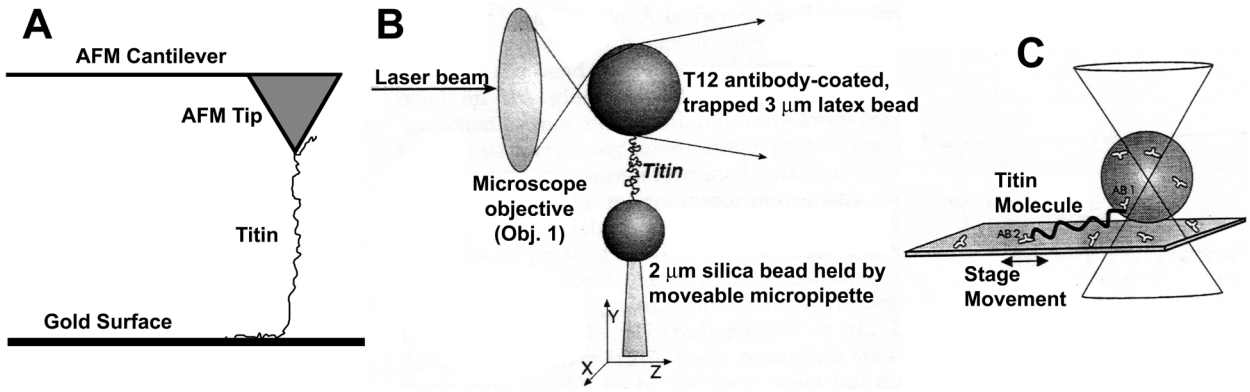

Fig.8: Wang, et al.